AN ANALYTICAL APPROACH TO UTILIZE TEMPERATURE AND PRESSURE PROFILE OF A MULTI-ZONE WELL IN ESTIMATING ZONAL FLOW CONTRIBUTIONS

A Thesis

by

ASIF AHMED

Submitted to the Office of Graduate and Professional Studies of
Texas A&M University
in partial fulfillment of the requirements for the degree of

MASTER OF SCIENCE

Chair of Committee,	Abu Rashid Hasan
Committee Members,	Jenn-Tai Liang
	M. M. Faruque Hasan
Head of Department,	Jeff Spath

August 2018

Major Subject: Petroleum Engineering

ABSTRACT

Oil and gas producers around the world face a major challenge in estimating zonal flow contributions in wells with multiple pay zones. This study develops an analytical approach that estimates zonal flow contributions from producing zones using the pressure and temperature profiles of the well. Such a method can assist operators to monitor wells and decide on workovers. This method can work best in an instrumented well that can provide real time pressure and temperature data.

This study develops a model that divides a multi-zone well into a series of producing and non-producing sections. Taking the mixing cup approach, energy and material balances are performed at the producing sections to quantify flow rate from the each reservoir. Measured pressure and temperature data from a well are used as the input of the model along with sand-face fluid temperature of each zone. Sand-face fluid temperature, when unavailable, is estimated using an analytical expression that relates reservoir flowing fluid temperature change with pressure drop and flow rate. The model is used first in the forward mode for a theoretical conventional dry gas well with multiple pay zones to generate synthetic pressure and temperature profiles along the wellbore for a given flow profile. Then the model is verified by using it in inverse mode with the generated synthetic temperature and pressure profile to estimate rates and error bounds. An iterative solution method is used as calculating sand-face temperature requires flow rate from the zone. Sensitivity study of the model is presented to show the relative significance of each variable. Sensitivity studies show that this model is highly dependent

on the accuracy of temperature measurements and that the model may not be useful for low producing zones.

Later, the model is applied to three field cases of gas wells from a conventional sandstone reservoir where producing zones are separated by impermeable shale layers. Spinner data from those wells are interpreted using a commercial software to generate a flow profile against which the model is validated. A recently developed analytical expression is used to estimate the unavailable sandface temperature. The quality of the match of the model estimates with spinner data is excellent. Limitation of the model in low producing zones is discussed.

DEDICATION

Two persons who taught me to stand in the ground and to reach for the stars.

My Parents Farah Diba Ahmed and Jalal Ahmed

ACKNOWLEDGEMENTS

I would like show my gratitude to my committee chair Dr. Abu Rashid Hasan for his guidance throughout the two years of my master's program. His intuitions has always helped me to try out different approaches which made this thesis possible.

I would also like thank my committee members Dr. Jenn-Tai Liang and Dr. M. M. Faruque Hasan for their support throughout the course of this research.

I acknowledge the support from Petrobangla by showing interest in my research and sharing field data to help me validate my research.

All my course teachers have been very helpful throughout last 2 years which helped me understand the bits of petroleum engineering. I would also like to appreciate the support I received from the department staffs which made my days here smoother.

I am grateful to Rayhana, Raka and rest of my friends at the department, who made my transition into graduate school from an industry job feel seamless and helped me perform my research.

Society of Petroleum Engineers Texas A&M University student chapter has been a big part of my two years in Aggieland. I would like to thank all the friends I made while working with SPE and appreciate the learning opportunity SPE has given me.

Special thanks to Bangladesh Students' Association for making me feel at home while staying 8500 miles away.

Finally, thanks to my parents and little brother for their encouragement.

CONTRIBUTORS AND FUNDING SOURCES

Contributors

Part 1, faculty committee recognition

This work was supervised by a thesis committee consisting of Dr. Abu Rashid Hasan [advisor] and Dr. Jenn-Tai Liang of the Department of Petroleum Engineering and Dr. M. M. Faruque Hasan of the Department of Chemical Engineering.

Part 2, student/collaborator contributions

All work for the thesis was completed independently by the student.

Funding Sources

There are no outside funding contributions to acknowledge related to the research and compilation of this document.

NOMENCLATURE

B_g	Gas formation volume factor, ft^3/Mscf
C_{JT}	Joule-Thomson coefficient, ft^3-°F/Btu
C_P	Specific heat capacity, Btu/lb_m-°F
c_g	Gas compressibility, psi^{-1}
c_t	Total compressibility, psi^{-1}
D or d	Tubing internal diameter, ft
f_f	Friction factor
g	Acceleration due to gravity, ft/s^2
g_c	Gravitational constant, 32.2 lb_m-ft/lb_f-s^2
g_G	Geothermal gradient,°F/ft
h	Formation thickness, ft
hc	Heat transfer coefficient, Btu/hr-ft^2
H	Enthalpy, Btu/lb_m
J	Conversion factor, 778 (ft-lb_f)/Btu
k	Permeability, mD
k_e	Thermal conductivity of formation, Btu/hr-ft-°F
L	Length of well segment, ft
L_R	Relaxation parameter, ft^{-1}
m(p)	Pseudopressure, psi
P or p	Pressure, psi

Q	Heat flow per unit length of wellbore, Btu/hr-ft
q	volumetric flow rate, Mscf/D
r	Radius, ft
r_{to}	Tubing outer radius, ft
N_{Re}	Reynolds Number
S	Saturation
s	Lumped parameter defined in equation (16)
T	Temperature, °F
T_{ei}	Undisturbed formation temperature, °F
T_D	Dimensionless temperature
t	Time, hr
v	Insitu fluid veloscity, ft/s
w	Mass flow rate, lb_m/s
Z	Z-factor of gas
z	Depth, ft
α	Inclination angle, °
γ	Specific gravity
ε	Surface roughness, ft
θ	Inclination angle, °
μ	Viscosity, cp
ν	Specific volume, ft^3/lb_m
ρ	Density, lb_m/ft^3

σ	Joule-Thomson throttling coefficient, Btu/lb_m-psi
ϕ	Porosity
φ	Lumped parameter defined in equation (19)

Subscripts

e	Formation or reservoir
f	Fluid
g	Gas
i	Initial
i	First node
j	Next node
n	Wellbore flow
p	Constant pressure
r	Reservoir flow
T	Constant temperature
w	Water
wf	Wellbore flowing

TABLE OF CONTENTS

Page

LIST OF FIGURES

Page

LIST OF TABLES

1. INTRODUCTION

1.1. Background

In the oil and gas industry, wells having multiple zone completions is a common incidence. Typically, a well is drilled in an area with multiple layers of reservoirs that can produce hydrocarbon. This leads to drilling and completing multiple reservoirs at the same time to maximize production in that well and to ensure faster recovery of resources. Being the most efficient way to produce from a field, such completions are highly prevalent in conventional wells around the world, especially in deep-water assets. But, multi-zone completions lead to a major challenge in estimating flow contributions from each zone. If the well has an expensive drilling program with formation tester, the reservoir pressures and other reservoir properties at each zone are known. But, when that well starts to produce, reservoirs starts to drain and reservoir pressure starts to deplete. Each zone is drained at a different pace due to a myriad of reasons and it gets difficult to estimate the flow from different zones from the surface. The problems created due to this can be enormous and expensive as the operator might be losing oil and gas to depleted zone from a producing zone (cross flow) or there might be significant water cut in one zone due to coning, affecting the production of the well. To solve such issues in a well, operators around the world perform well surveillance in many forms and take on workover projects when deemed as the only solution to the problem. Workover projects are expensive and the opportunity cost of each decision in a workover project can be significant. As the world

moved to more matured fields and older wells, the importance of zonal flow allocation is of prime importance now.

Traditionally, for well surveillance and well monitoring, production logging has been the main source of estimates of zonal flow contributions. There are different types of production logs that can be run for various purposes and multiple types of log can be run in tandem to get a plethora of measurements that assist the operators in diagnosing different kinds of issue. Over the years, the use of production logging has grown significantly and it now encompasses the whole lifecycle of a well from drilling days to well abandonment.

Use of production logging can be traced back to early days of the industry when temperature surveys were introduced as a mean of finding fluid entry points in a wellbore. The industry during those days figured from the idea of Joule-Thompson cooling that a colder temperature anomaly can be detected in a zone where gas is coming into the wellbore and expanding (Schlumberger et al 1937). Then, in the 1940s, the industry saw the introduction of spinner flowmeters and pressure surveys which added more information about the well conditions. Pressure gradients gave the industry a way to identify the fluid type and the flowmeters gave a more direct measurement of the flow rate at different depths. (Millikan, 1942 & Dale, 1949).

As a field engineer, I had the privilege to run production logs and help clients around the world to diagnose issues in their wells. Although, the common perception of production logging is that it is easier compared to major activities like drilling and

completion, planning and execution of production logging can be a herculean effort. As well intervention methods like wireline or slickline are required to perform production logging, it takes weeks of prior planning and mobilization. Coiled tubing operation can get involved if the deviation of a well is really high. In spite of all the expenses and challenges, production logging can give an operator many insight on the wellbore status. The most common form of production log these days include temperature, pressure, density and spinner flowmeter measurements at a minimum. In case of multi-phase wells, we see other sensors like capacitance, gradiometer etc. For many reasons, these different logs can be used in combination to indirectly estimate an unknown parameter or can be used to compare between interpretations of each type of log. Modern production logging tool has become compact and can accommodate more sensors in a short tool string to facilitate the industry's need of estimating flow contributions from zones in a well. But, with all its benefits, production logging gives us measurement only when it is run in a well, thus it is not a continuous source of data.

As mentioned in previous paragraphs, simple temperature logs have also been used for zonal flow contribution estimates for a long time in the industry which can give good estimates of the flow profile in multi-zone well. With latest developments in Distributed Temperature Sensors (DTS) and Distributed Pressure Sensors (DPS), operators now have access to real-time continuous high-frequency data to have really accurate temperature and pressure profiles for a well. Optical fiber sensors started to be introduced in the oil and gas industry in the early 90s (Lequime et al, 1991). These devices took an existing communication technology from telecommunication industry and exploited it to use in

oilfields (Grattan et al, 1995). Early tests of such optical fiber sensors can be found in the works of Karaman et al (1996) who tested the data quality and reliability of such temperature and pressure sensors at West Coalinga Field in California. They found an excellent correlation with conventional temperature measurement. A similar correlation was seen with DPS sensors and two other conventional pressure gauges. Brown and Hartog (2002) discussed the capabilities and applications of such sensors. They concluded that accuracy of up to 0.1°C can be achieved in such distributed temperature sensors and optical fiber sensors can have the potential for use in well surveillance in offshore wells where operators are not inclined to perform a regular well intervention.

Although these technologies have not seen widespread use yet, we are seeing more and more of such sensors in wells around the world, more commonly in deep-water assets. Access to such data allows us to infer information about the well continuously and perform real-time well surveillance. Estimating zonal flow contributions from temperature and pressure profiles in real-time, by not hampering well production schedule for well intervention projects such as production logging, can be a big relief for operators around the world. So, development of improved and simpler ways to zonal flow allocation through temperature and pressure profile is significant considering where the oil and gas industry is headed.

1.2. Research Objective

The objective of this study is to utilize temperature and pressure profiles from logging or distributed sensors to estimate zonal flow contributions in an analytical

approach. To do that, we have performed energy and mass balance in a control volume within the wellbore, which led us to a generalized algebraic expression which can be used to generate a flow profile. This approach can be considered more robust than usual temperature logging interpretation as it accounts for all kinds of energy changes. In addition, being an algebraic expression, this method offers a simple solution for estimating zonal flow contribution requiring minimal experience interpreting such data. The developed model also takes the temperature of the inflow fluid into account which can be measured in a well-instrumented with sand-face temperature sensors. When such sand-face temperature sensor is unavailable, the sand-face fluid temperature can be calculated from a recently developed analytical model.

In this study, we have taken a forward modelling to generate a synthetic dataset of temperature and pressure throughout a theoretical conventional dry gas well section. Later, the model was used to estimate the flow rate of the theoretical well section utilizing the synthetic dataset. To use the model, an iterative method was developed as zonal flow rate is required to calculate sand-face fluid temperature. Then, a set of sensitivity analysis was performed on each parameter to find out the comparative significance of each variable on the output flow profile and discuss how the data measurement and utilization for this model can be done most efficiently.

Finally, the model is checked against 3 field case studies from 3 conventional dry gas wells. Each case study includes 3 different cases of different surface flow rates. Production logging raw data for each of those cases are interpreted using a commercial

software to get a flow profile. Later, the model is validated against the interpreted flow profile. The workflow of using the model in such real-world cases are discussed and the inaccuracies in the output are explained. The process of using this model is explained in detail so that it can be replicated and can be used for any well with minor changes.

1.3. Literature Review

To go ahead with the research objective discussed in the previous sub-chapter, the studies done this field prior to our attempt was reviewed. As the primary variable for the intended model is temperature measurement along the wellbore length, the history of temperature logging interpretation for zonal flow allocation is relevant. In the background sub-chapter, it was mentioned that temperature logging have been part of the oil and gas industry for decades. Many methods of temperature log interpretation has been discussed in numerous papers dated back to 1950s. Nowak (1953) and Bird (1954) did some early work on interpretations of temperature logs to estimate zonal flow contributions for injection wells and gas producing wells. Bird used his simple interpretation method to interpret zonal flow allocation for a gas producing well. Bird and Frost (1965) and (1966) continued on their previous work showing few more field examples estimating flow profiles in the wellbore.

Following them, temperature log interpretation was investigated by many authors in next two decades. Kunz and Tixier (1955) expanded on the existing idea and validated with multiple field case studies. They developed a method for the investigation of gas

producing wells where they used temperature log as primary input and needed radioactivity and induction logs as auxiliary documents.

Schonblom (1961) expanded the research done before and discussed many scenarios faced in evaluating flow profile in a multi-pay well. He developed a new relationship avoiding some of the simplifying assumptions made by his predecessors in this field of study. He concluded that temperature measurement can end up being a source of quantitative zonal flow rate allocation.

Peacock (1965) compiled and discussed different methods of temperature log interpretation and usage of the interpreted information. Kading and Hutchins (1969) showed the use of temperature log for different purposes, for example evaluating fracture or acid job, water injection wells etc.

Romero-Juarez (1969) developed a simple expression that allows allocating flow to each zone using temperature profile of the well. This expression has been widely used over the world for a long time and still taught as one of the prominent methods of quick temperature log interpretation.

Curtis and Witterholt (1973) connected simple models of heat exchange phenomena associated with temperature logging which includes Ramey's (1962) seminal work in wellbore thermal model. Through this, they proposed a better understanding of temperature log interpretation and suggested that temperature logging should be utilized in conjunction with spinner logs for a better approximation of actual flow rates from each

zone. They also discussed some conditions which they believed to be the best conditions for estimating flow contributions from producing zones.

Steffenson and Smith (1973) discussed the effect of Joule-Thomson effect of the fluid in details. Joule-Thomson effect becomes very significant in large pressure drawdowns from reservoir and wellbore. In later years people continued to work on methods and field case studies of estimating zonal flow contribution utilizing temperature logs but major innovation did not take place until the introduction of distributed temperature sensors.

The introduction of distributed temperature sensors (DTS) and distributed pressure sensors (DPS) has brought a paradigm shift in the industry. Developments in the field of optical fiber have made such sensors so efficient that can be very accurate. In present day, DTS accuracy can reach to the range of 1°C and resolution can reach the range of 0.01°C (Halliburton Brochure, 2012), which is on par with modern production logging tools. Also, with fixed optical fiber setup inside the well, movements of sensors can be eliminated. Movements in the sensors introduces error in production logging tool temperature measurements due to the lag of the sensor. The usage of such distributed sensors have risen significantly in the last decade, and now we see them being heavily used in unconventional shale gas wells due to the value they add to production surveillance and monitoring, monitoring hydraulic fracturing and, acidizng jobs etc. With more and more DTS and DPS being installed around the world, operators suddenly have access to huge amount of good quality continuous data in real-time that is waiting on interpretations. So,

the need of better empirical and physics based models for production monitoring has recently gained importance again.

One of the first works in this field was done by Ouyang and Belanger (2006). They developed a thermal wellbore model and used the model for flow profiling using a forward modelling approach to match the temperature profile from DTS. They observed that it is difficult to use DTS data in multiphase wells as DTS does not provide pressure, density or holdup data. But, DTS data can be used successfully for single phase wells. A very important finding from there research is that at a deviation of more than 75°, change in temperature is very minute as the geothermal temperature is not changing significantly. They concluded that below that threshold, DTS temperature measurements can be used for flow profiling with accuracy.

Brown (2006) has shown that a robust flow and thermal model can accurately estimate flow contributions from zones in a multilayered well. He utilized simple temperature log interpretation and a more robust model in his method. He showed that reservoir properties can be approximated from his model as long as a baseline data is obtained at an early stage of production when the reservoir data is known. This method then can be used to estimate drawdowns in each zone and significant increases in GOR. In his paper, he also showed a comparison with spinner log to compare the flow profile from his model.

Johnson et al. (2006) showed that use of DTS technology can a be cost effective solution for operators to identify water breakthrough. They discussed the importance of

continuous flow profiling by using DTS data and showed field case studies to validate their claim. They also showed DTS vs PLT comparisons to solidify the idea of installing DST as long-term solution for well monitoring.

Kabir et al. (2008) showed the use of DTS temperature in predicting flow rate from the top of perforations to the surface independent of any surface information. Later Wang et al. (2010) expanded said work and used Fourier series approximations to match DTS traces which resulted in better accuracy while preserving spatial resolution. They showed with two gas well examples that, multipoint pressure measurement can be used in tandem with DTS data for flow profiling and the resulting flow profile is more accurate.

Muradov and Davies (2012) presented a study of the allocation of flow rate from different zones using classical asymptotic temperature interpretation method of DTS data. Their study concludes that this method is pretty accurate when it comes to estimating zonal contributions.

Yoshioka et al. (2005) developed a coupled wellbore-reservoir model for horizontal wells with DTS measurements. They found that temperature and pressure profiles are sensitive to well trajectory and a good well directional survey is required for the accuracy of their model. A significant finding in their work was that clearly detectable discontinuities in the slope of temperature profile denote a change in fluid. Their model works best in high flowing oil wells and gas wells. Later in their research, Yoshioka et al. (2007 & 2009) presented an inversion technique to interpret DTS measurements. The basic idea of their method was using Levenberg-Marquardt algorithm to minimize error

in flow profile estimation. They presented validation of their model using synthetic data and field case studies from North Sea horizontal oil wells. Barrette et al. (2012) also estimated field flow profile from measured temperature and pressure through inverse problem method and verified it with spinner data.

Venkataraman et al. (2015) presented a simple model for obtaining flow contribution from several producing reservoir sections using temperature and pressure measurements available from sensors placed over the length of a producing well. They showed a field case study of a deep-water oil well. Later, Hasan et al. (2017) have taken a similar approach in developing an analytical model validated against synthetic data and available multiphase field case studies.

2. MODEL DEVELOPMENT

This chapter discusses the development of an analytical model to estimate the flow rate contribution from individual zones in a well with multiple pay zone completion. The model was developed by having a conventional gas well in consideration, but it can be utilized for any well with minimal modification, if any. The model considers fluid flow and heat transfer in the wellbore and performs energy and mass balance using the mixing cup approach. Following sub-chapters will discuss the major assumptions that were taken into account to develop the model, the typical wellbore design that was being considered for the model, and the derivation of the analytic solution.

2.1. Model Assumptions

To develop the model, several simplifying assumptions were made. Following bullet points discusses the significant assumptions,

1. Steady state flow was considered within the wellbore.
2. No fluid from the wellbore is flowing outside to any reservoir.
3. It was assumed that each of the pay zones are homogeneous reservoirs with constant reservoir properties in any direction from the wellbore to reservoir boundary.
4. Reservoir temperature and initial pressure were assumed to be constant for each zone.
5. Each individual pay zone was considered to have a constant production rate.

6. Fluid entering radially from reservoir and fluid from the non-producing zone below were assumed to be mixing instantaneously and reaching thermal equilibrium before exiting into the next non-producing zone.
7. The model neglects any heat generated due friction with wellbore wall.
8. Production fluid from a zone and the wellbore flowing fluid from the zones below were assumed to have same composition.
9. Fluid properties were assumed to remain constant at any particular point in the wellbore, but varied with the depth due to the change in temperature and pressure.
10. Specific heat capacity was assumed to stay constant throughout the section of interest as the variation is usually negligible.

2.2. Model Development for Single Phase Gas

To develop the model, a typical conventional wellbore is considered that is producing from multiple pay zones. The wellbore is divided into a series of producing wellbore sections and non-producing wellbore sections. At the deepest point of the well, only the incoming fluid from the deepest pay zone exists. From that point, fluid is flowing upwards towards the surface through the wellbore. In subsequent producing sections, reservoir fluid comes into the wellbore and mixes with the fluid that is already flowing upwards and continue to flow. Following schematic diagram shows the typical well used for our model,

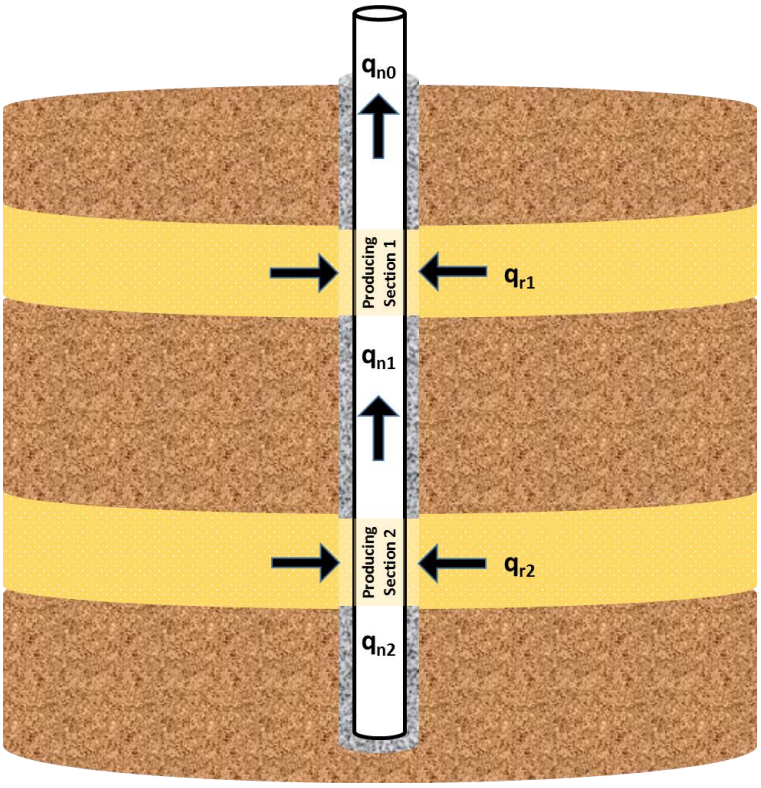

Figure 1: Schematic of a typical wellbore system

The objective in this subchapter is to develop an analytic expression for single-phase gas that defines the production rate from a certain pay zone using the temperature and pressure data from the wellbore and sand-face fluid entry temperature and pressure data. To develop that expression, we started from a basic energy balance for a control volume in the wellbore.

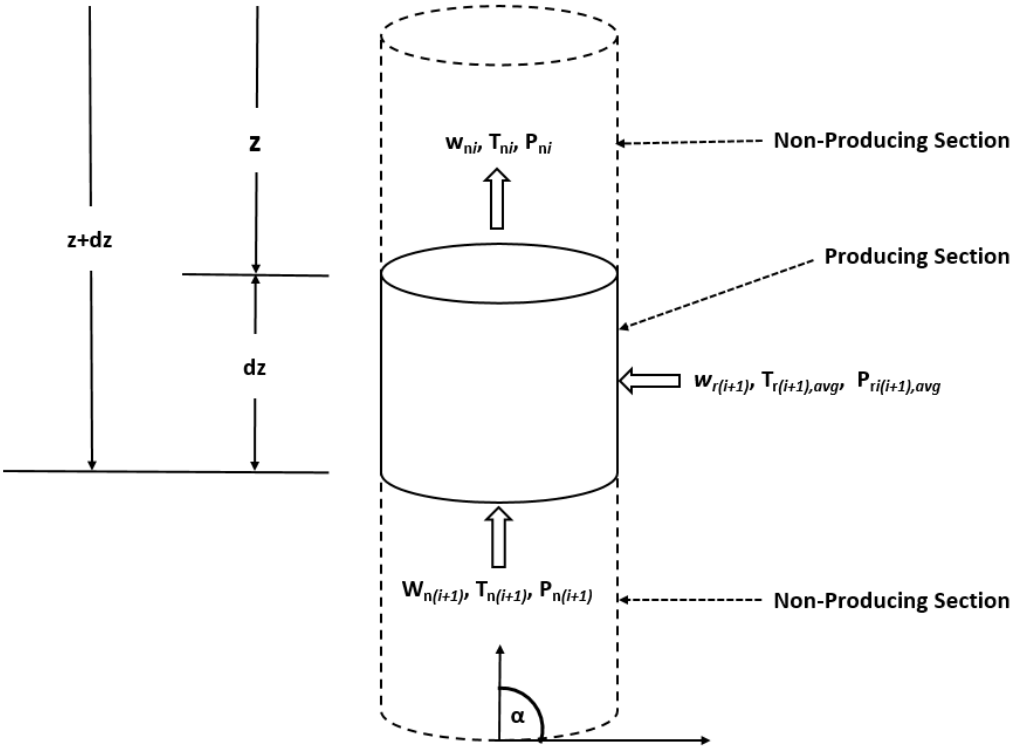

Figure 2: Schematic of a well showing a producing section between two non-producing section

Figure (2) shows a cut section for the typical well discussed in the previous section. The dotted cylinder is the wellbore section in consideration which has a producing section stacked between two non-producing sections. The producing section in the figure (2) is producing from the reservoir (i+1). The solid line cylinder within the wellbore cut section is the control volume where we performed energy balance. This cylindrical control volume has a radius of r_w feet and height of dz feet. The control volume (or the wellbore cut-section in consideration) is inclined at an angle of α° to the horizontal plane.

Single phase fluid is entering the control volume from the bottom face at a rate of $w_{n(i+1)}$ (lb_m/day) at a temperature $T_{n(i+1)}$ (°F) and the pressure at that point is $P_{n(i+1)}$ (psi). Measured depth at this point is (z+dz) from the surface. This fluid mixes with the fluid that is entering the control volume from the reservoir (i+1). The rate of fluid entering from reservoir is $w_{r(i+1)}$ (lb_m/day) at a sand-face entry temperature $T_{r(i+1),avg}$ (°F) and the pressure at that point is $P_{n(i+1),avg}$ (psi). As per the assumption made in section 2.1, both incoming stream into the control volume mixes instantaneously and moves upwards to exit the control volume at measured depth z. Flow rate at exit point is w_{ni} (lb_m/day) at a temperature T_{ni} (°F)and the pressure at that point is P_{ni} (psi).

Now, if an energy balance is performed for the defined control volume, considering the change in enthalpies of each fluid stream, and their kinetic and potential energy, we get the following expression,

$$w_{n(i+1)}\left(H_{n_{(z+dz)}} - \frac{g(z+dz)sin\alpha}{Jg_c} + \frac{v^2_{n_{z+dz}}}{2Jg_c}\right) + w_{r(i+1)}\left(H_{r_{\left(z+\frac{dz}{2}\right)}} - \frac{g(z+\frac{dz}{2})sin\alpha}{2Jg_c} + \frac{v^2_{r(i+1)}}{2Jg_c}\right) + Qdz = w_{ni}\left(H_{n_z} - \frac{gzsin\alpha}{Jg_c} + \frac{v^2_{n_z}}{2Jg_c}\right) \ldots\ldots\ldots (1)$$

Equation (1) above has the terms $w_{n(i+1)}H_{n_{(z+dz)}}$and $w_{r(i+1)}H_{r_{(z+dz/2)}}$, which are the enthalpies for the fluid entering the control volume from the non-producing section (i+1) below and from the reservoir (i+1) respectively. Similarly, $w_{ni}H_{n_z}$ is the enthalpy for the fluid exiting the control volume to the non-producing section (i).

In the left side of equation (1), terms $\left(w_{n(\mathrm{i}+1)}v_{n_{z+dz}}^2\right)/(2Jg_c)$ and $\left(w_{r(i+1)}v_{r(i+1)}^2\right)/(2Jg_c)$ represents the kinetic energy of the incoming fluid from deeper zones and reservoir (i+1) and the terms $\left(w_{n(\mathrm{i}+1)}g(z+dz)sin\alpha\right)/(Jg_c)$ and $\left(w_{r(\mathrm{i}+1)}g(z+dz/2)sin\alpha\right)/(Jg_c)$ are the potential energies of the incoming fluid from deeper zones and reservoir (i+1). In the right side of equation (1), terms $\left(w_{ni}v_{n_z}^2\right)/(2Jg_c)$ and $(w_{ni}gzsin\alpha)/(Jg_c)$ represents the kinetic energy and the potential energy of the exiting fluid. The constants *J* and g_c in those terms are unit conversion factors which are used to bring the energy terms in equivalent units. Contributions from kinetic energy is neglected as it is negligible compared to the rest of the energy terms in the equation. Finally, the term Qdz is the heat lost to or gained from the surroundings from the control volume with positive value meaning heat gained.

If a mass balance is performed in the control volume, then the incoming fluid mass into the control volume from the wellbore below and the reservoir has to add up to be the fluid mass leaving the control volume. So,

$$w_{ni} = w_{n(i+1)} + w_{r(i+1)} \dots\dots\dots (2)$$

Combining equations (1) and (2),

$$w_{n(\mathrm{i}+1)}\left(H_{n_{(z+dz)}} - \frac{g(z+dz)sin\alpha}{Jg_c}\right) + \left(w_{ni} - w_{n(\mathrm{i}+1)}\right)\left(H_{r_{\left(z+\frac{dz}{2}\right)}} - \frac{g(z+\frac{dz}{2})sin\alpha}{2Jg_c}\right) +$$

$$Qdz = w_{ni}(H_{n_z} - \frac{gzsin\alpha}{Jg_c}) \dots\dots\dots (3)$$

In this model, single phase gas flow is considered. There are no phase change or reaction, and the mixing is isoenthalpic. In such a condition, from classical thermodynamics, change in enthalpy is dependant on change of temperature and pressure in the fluid. The general term defining the change in enthalpy is,

$$dH = \left(\frac{\partial H}{\partial T}\right)_P dT + \left(\frac{\partial H}{\partial T}\right)_T dP$$

$$dH = C_P dT + \left[v - T\left(\frac{\partial v}{\partial T}\right)_P\right] dP$$

$$or, dH = C_P dT - C_{JT} C_P dP \ldots\ldots\ldots (4)$$

The term C_{JT} represents the Joule-Thomson coefficient and C_P is the specific heat capacity of the fluid. To calculate Joule-Thomson coefficient for real gases, following expression can be used if C_P is known for the fluid,

$$C_{JT} = \frac{1}{C_P}\left(\frac{vT}{Z}\right)\left(\frac{\partial Z}{\partial T}\right)_p \ldots\ldots\ldots (5)$$

The last term in the left side of the equation (1) is Qdz, which is the heat added to fluid from the formation over the length of the control volume. Within this term, Q is the heat transfer rate per unit length of wellbore. The value of Q can be approximated using the following equation developed by Hasan and Kabir (2002),

$$Q = -L_R w C_P\left(T_f - T_{ei}\right) \ldots\ldots\ldots (6)$$

In equation (6), T_{ei} is the formation temperature at the depth of the control volume in consideration and L_R is the relaxation length parameter. L_R is the inverse of an parameter A, which was defined by Ramey (1962) and acts as an overall heat transfer coefficient of sorts that gives the heat transferred from the formation to the fluid over a unit length of wellbore. This relaxation length parameter is defined mathematically as the following expression by Hasan et al. (2002),

$$L_R \equiv \frac{2\pi}{C_P w}\left[\frac{r_{to}U_{to}k_e}{k_e + (r_{to}U_{to}T_D)}\right] \dots\dots\dots (7)$$

Now, let us consider that $c_{p_{n(i+1)}}$ and $c_{p_{r(i+1)}}$ are the heat capacity of the fluid that is flowing into the control volume from the wellbore below and from the reservoir (i+1). And c_{p_n} is the heat capacity of the fluid leaving the control volume. Additionally, another assumption states that the entering fluids from each reservoir has same composition. So, it can be assumed that heat capacity of the each fluid stream is same. Mathemetically expressing the statements above, we get,

$$C_{P_{n(i+1)}} = C_{P_{ni}} = C_{p_{r(i+1)}} = C_P \dots\dots\dots (8)$$

Combining equation (3), (4) and (8),

$$w_{n(i+1)}C_P\left(\left(T_{n(i+1)} - T_{r(i+1),avg}\right) - C_{JT}\left(P_{n(i+1)} - P_{r(i+1),avg}\right) - \frac{g\left(\frac{\Delta z}{2}\right)sin\alpha}{C_P J g_c}\right) +$$
$$w_{ni}C_P\left(\left(T_{r(i+1),avg} - T_{ni}\right) - C_{JT}\left(P_{r(i+1),avg} - P_{ni}\right) - \frac{g\left(\frac{\Delta z}{2}\right)sin\alpha}{C_P J g_c}\right) = -Qdz \dots\dots\dots (9)$$

Qdz is very small for a typical reservoir height and can be considered negligible. So, we can simplify equation (9) to the following expression,

$$w_{n(i+1)} = w_{ni}\frac{\left(T_{ni} - T_{r(i+1),avg}\right) - C_{JT}\left(P_{ni} - P_{r(i+1),avg}\right) + \frac{1}{2}\frac{g\Delta z sin\alpha}{C_P J g_c}}{\left(T_{n(i+1)} - T_{r(i+1),avg}\right) - C_{JT}\left(P_{n(i+1)} - P_{r(i+1),avg}\right) - \frac{1}{2}\frac{g\Delta z sin\alpha}{C_P J g_c}} \ldots\ldots\ldots (10)$$

If the standard condition flowrates at depth z and (z+dz) are q_{ni} and $q_{n(i+1)}$ and the fluid density is ρ then,

$$q_{n(i+1)} = \frac{w_{n(i+1)}}{\rho} \ldots\ldots\ldots (11)$$

$$and \quad q_{ni} = \frac{w_{ni}}{\rho} \ldots\ldots\ldots (12)$$

Combining equations (10), (11) and (12), we get,

$$q_{n(i+1)} = q_{ni}\frac{\left(T_{ni} - T_{r(i+1),avg}\right) - C_{JT}\left(P_{ni} - P_{r(i+1),avg}\right) + \frac{1}{2}\frac{g\Delta z sin\alpha}{C_P J g_c}}{\left(T_{n(i+1)} - T_{r(i+1),avg}\right) - C_{JT}\left(P_{n(i+1)} - P_{r(i+1),avg}\right) - \frac{1}{2}\frac{g\Delta z sin\alpha}{C_P J g_c}} \ldots\ldots\ldots (13)$$

Equation (13) works as the model for sequentially estimating flow rates from individual control volumes (or in macro scale, individual zones) if the flow rate above the shallowest producing section is known. In practical scenarios, the surface flow rate is known, which is the same as the flow rate exactly on the top of the shallowest perforation or producing section. Thus, knowing this q_0, we can go forward and sequentially estimate q_1, q_2, q_3 and so on if all the parameters on the fraction in the right side of equation (13) is measured and/or estimated correctly.

3. VALIDATION USING SYNTHETIC DATASET

To validate the model that was developed in the previous chapter, we decided to develop a synthetic set of data for a theoretical well that represents the type of well we have for the field case studies. The procedure of generating this set of synthetic data involves calculating pressure and temperature in different points of wellbore in short intervals from assumed flow rates from different pay zones using published and well established analytical methods. The objective for this chapter is to generate a dataset in a simple non-confounding way to test the model before moving on to field case studies which bring various uncertainties into the estimation.

3.1. Model Well for Data Generation

A simple model well section is assumed to generate pressure and temperature data along the wellbore. Figure (3) shows a simple schematic of the model well section in consideration. All assumptions made in subchapter 2.1 are considered valid while generating synthetic data to verify the model.

This model well is a vertical well section from measured depth of 8000 ft up to 6000 ft. Pressure, temperature, and flow rate is known at 8000 ft. The fluid flowrate in the upward direction at this point is 5000 Mscf/D. Temperature and Pressure of the fluid at this point is assumed to be 182 °F and 2000 psi. The model well section has 3 payzones named P, Q and R. Table (1) shows the basic information for those pay zones. It was

assumed that the fluid in the wellbore and the produced fluid from the payzones have a specific gravity of 0.6.

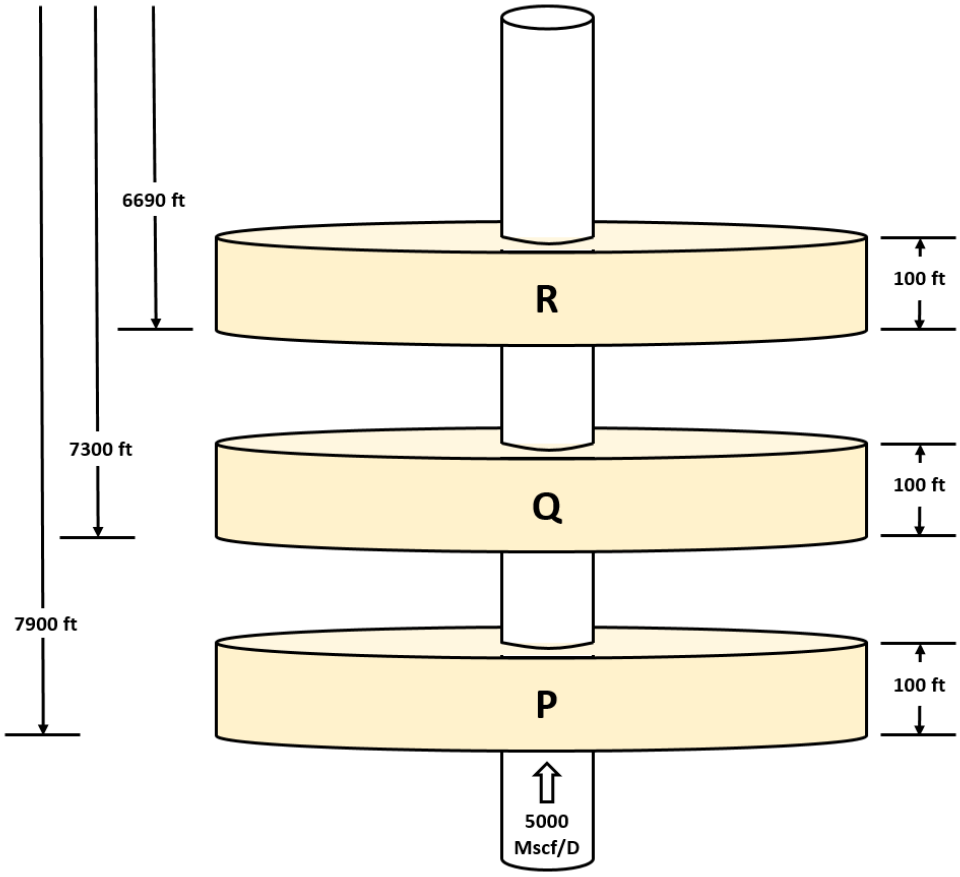

Figure 3: Schematic of the model well assumed for synthetic data generation

Table 1: Reservoir information for the model well assumed for synthetic data generation

Payzone	Depth (ft)	Reservoir Radius, Re (ft)	Average Reservoir Pressure, Pe (psi)	Reservoir Geothermal Temperature, Tei (degF)	Gas Inflow from Reservoir, q (Mscf/d)
P	7800-7900	4000	2420	178.55	12500
Q	7200-7300	4000	2260	172.55	20000
R	6590-6690	4000	2240	166.45	7500

Following Parameters were kept constant for each of the zones while generating the dataset,

Table 2: Input parameters for the payzones

Input Parameter	Value	Unit
Gas Specific Gravity, γ_g	0.6	
Formation Density, ρ_{form}	165.4	lb/ft^3
Formation Specific Heat, $c_{p\text{-}form}$	0.2	$Btu/lb.°F$
Reservoir Radius, r_e	4000	ft
Heat Transfer Coefficient, h_c	1	$Btu/hr - ft^2°F$
Production time, t	1	days

3.2. Pressure and Temperature Profile of the Model Well

3.2.1. Pressure Profile Data Generation

To generate a pressure profile, we started at the bottom of model wellbore section where the fluid pressure is known. Pressure at this point (at 8000 feet measured depth) is considered to be P_1. Then an analytical approach is utilized to calculate the pressure drop in the wellbore for single phase compressible Newtonian fluid. The approach used is discussed in details in 'Petroleum Productions Systems' book by Economides et al (2013). In this approach, following expression is used to calculate pressure in 10 feet intervals.

$$p_2^2 = e^s p_1^2 + 2.685 \times 10^{-3} \ \frac{f_f(\bar{Z}\bar{T}q)^2}{\sin\theta \, D^5} \ (e^s - 1) \ldots\ldots\ldots (15)$$

$$where, \ \ s = \frac{-0.0375\gamma_g \sin\theta \, L}{\bar{Z}\bar{T}} \ \ldots\ldots\ldots (16)$$

The fluid properties required in both equations are calculated using the known pressure and tempurature at 8000 feet and are utilized to get P_2 which is the pressure at a point 10 feet above or at 7990 feet. Using calculated pressure and temperature (temperature calculation procedure discussed in next subchapter) at 7990 feet, fluid properties at that depth was calculated and pressure at 7980 feet was calculated. These steps can be continued to get the pressure profile for the model well section.

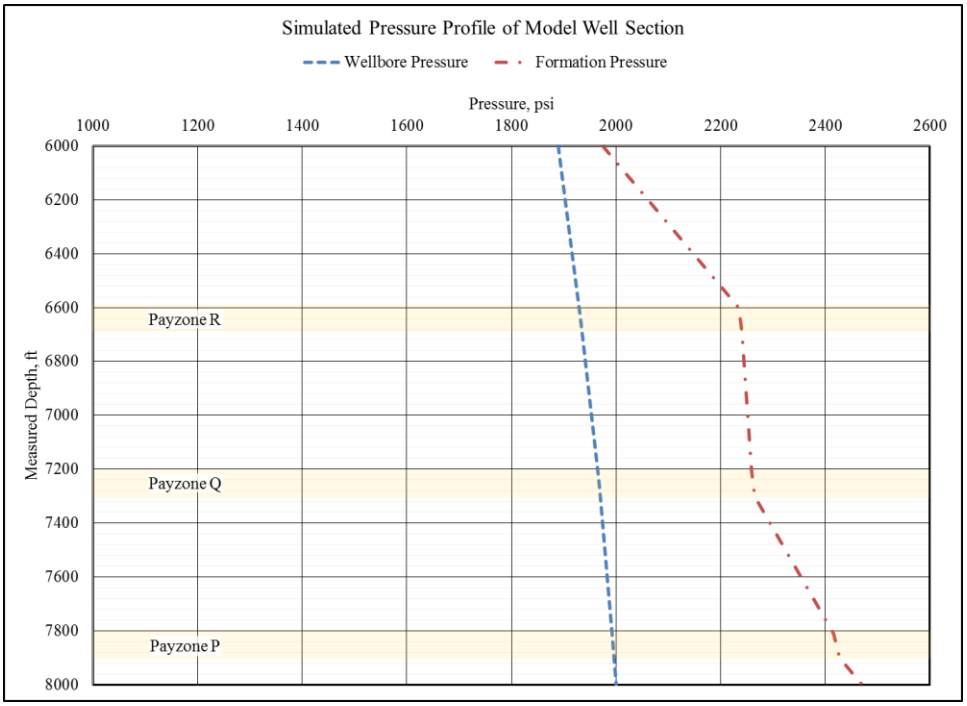

Figure 4: Generated synthetic pressure profile for the model well section

Accuracy of the calculation can be improved by having smaller intervals and using average of fluid properties from the points on either of that interval by running another iteration of this step. But, 10 feet interval was significantly small which meant the change in fluid properties is very small in each interval. A sample calculation is shown in

Appendix A for pressure and temperature calculation. Figure (4) shows the simulated pressure profile the model well section.

3.2.2. Temperature Profile Data Generation

To generate a temperature profile, we started at the bottom of model wellbore section where the fluid temperature is known. Temperature was calculated sequentially moving upwards at 10 feet intervals. Temperature calculation in this wellbore is complex as there are multiple producing sections which are preceded and followed by non-producing sections. As gas from reservoir is coming into the wellbore in producing sections, fluids of different temperature are mixing. In addition, Temperture of the reservoir inflow has to be estimated in order to perform mixing cup calculations. These steps make temperature profile calculation much more complex than pressure profile. Following subchapters will discuss the computation steps mentioned in this section in details.

3.2.2.1. Temperature Profile Data Generation in Non-Producing Sections

For the non-producing sections in the model well, Hasan et al. (2009) approach was utilized, which is a robust steady-state model for flowing fluid temperature in a complex well. Although the model well is fairly simple in design and assumptions, this approach gives a generalized expression that can be usable in any well having complex designs. In reality, wells might have changing geothermal gradient with depth, variable inclination and completion structure. The analytical approach developed by Hasan et al.

can be utilized in all such cases and thus helps our synthetic data generation method to be more robust.

Hasan et al. (2009) has shown that, the gradient of flowing fluid fluid temperature in a well can be expressed by the following expression which was derived from performing a general energy balance within a inclined well production system,

$$\frac{dT_f}{dz} = C_J \frac{dp}{dz} + \frac{1}{C_P}\left[\pm\frac{Q}{w} + \frac{g\sin\alpha}{Jg_c} - \frac{v}{Jg_c}\frac{dv}{dz}\right] \quad \ldots\ldots\ldots (17)$$

This expression can be simplified replacing Q from equation (4) developed by Hasan et al. (2002) to express the amount of heat gained by the fluid from the formation,

$$\frac{dT_f}{dz} = \pm L_R\left(T_f - T_{ei}\right) + \frac{g\sin\alpha}{C_P J g_c} - \varphi \quad \ldots\ldots\ldots (18)$$

$$where, \qquad \varphi = \frac{v}{C_P J g_c}\frac{dv}{dz} - C_J\frac{dp}{dz} \quad \ldots\ldots\ldots (19)$$

For a well that has multiple sections with different inclination angle α, or different geothermal gradient, or in our case a non-producing section after each producing section, Hasan et al. (2009) expanded equation (18) to the following form,

$$\frac{dT_f}{dz} = \pm L_R\left(T_f - z g_{Gi}\sin\alpha_j\right) \mp \pm L_R\left(T_{ei_j} - L_j g_{Gj}\sin\alpha_j\right) + \frac{g\sin\alpha_j}{C_P J g_c} - \varphi \quad \ldots\ldots\ldots (20)$$

In equation (20), the subscripts *j* denotes different depths of the wellbore. The point to be noted for this equation is that any term with subscript *j* is the value of that parameter at

the depth L_j and stays constant for that section of the well. Solving equation (20) as it becomes a first-order linear differential equation due to considering all parameters except T_f to be invariant with respect to depth variable z, following expression can be derived,

$$T_f = T_{ei} + \frac{1 - e^{(z-z_j)L_R}}{L_R}\left(g_{G_j}\sin\alpha_j + \varphi - \frac{g\sin\alpha}{C_P}\right) + e^{(z-z_j)L_R}(T_{f_j} - T_{ei_j}) \dots\dots\dots (21)$$

Utilizing this equation, temperature profile of a non-producing section in a complex well structure can be estimated. For, the model well section, fluid temperature was calculated using equation (21) sequentially at 10 feet steps moving upwards.

3.2.2.2. Data Generation of Sand-Face Temperature in Producing Section

In the producing section of a well, there are perforations or other kinds of completions that allow fluid to come into the wellbore from the surrounding reservoir. For our model, the temperature of this inflow fluid is required at the point of entry which is the sand-face. This sand-face fluid temperature can be significantly different from the known geothermal temperature at that depth. The reason behind this is Joule-Thomson cooling or heating of the fluid. As soon as a well is flown, fluid throughout the drainage radius of the reservoir moves towards the wellbore. During this flow through porous media, the fluid pressure decreases which result in Joule-Thomson cooling or heating of the fluid. Although, the Joule-Thomson effect can be smaller for low-pressure drawdowns and liquid fluid, for high-pressure drawdowns and for gas, the effect can be significant.

In reality, it is challenging to measure this sand-face fluid temperature correctly as it is very difficult to install a temperature sensor/optical fiber in a way that gives us the accurate measurement of the fluid temperature exactly at the sand-face. As soon as the fluid enters the wellbore, it starts to mix with fluid that is already inside and the temperature starts to change. So, a sensor at any point inside the well bore will not give the correct estimation of sand-face temperature. Therefore, for this research work, a recently developed analytical model by Xu et al. (2018) was utilized to generate synthetic data for the sand-face temperature at the producing sections of the model wellbore. This model takes nonisothermal behavior, adiabatic expansion (neglected in fully analytical solution), heat convection and heat exchange with surrounding formation into account. The following expression shows the fully analytical solution of the model that was used in this thesis,

$$T(r,t) = T_{ei} + \frac{C}{2B} e^{\frac{Dr^2}{2B}} Ei\left[-\frac{D(Ar^2+2Bt)}{2AB}\right] - \frac{C}{2B} e^{\frac{Dr^2}{2B}} Ei\left[-\frac{Dr^2}{2B}\right] \quad \ldots\ldots\ldots (22)$$

In the left side term, r represents the distance of the point from wellbore center in radial direction and t is the time of production in hours. Thus, this expression allows us to estimate temperature at point at any distance from the wellbore and at any time. Ei in the expression represents the eigen function A, B, C and D are constants which can be calculated using following equations,

$$A = \left[\emptyset S_g \rho_g C_{P_g} + \emptyset S_w \rho_w C_{P_w} + (1-\emptyset)\rho_e C_{P_e}\right]\left(\frac{2\pi h}{q}\right) \quad \ldots\ldots\ldots (23)$$

$$B = \rho_g C_{P_g} \ldots\ldots\ldots (24)$$

$$C = \frac{q\rho_g \sigma_g \mu_g}{2\pi hk} \ldots\ldots\ldots (25)$$

$$D = \frac{4h_c \pi}{q} \ldots\ldots\ldots (26)$$

σ_f is the fluid throttling coefficient and it is related to J-T coefficient by the following relationship,

$$\sigma_f = -C_{JT} C_{P_g} \ldots\ldots\ldots (27)$$

In equations (23) to (26), $\emptyset$ is the porosity of the formation, h is the formation thickness, h_c is the heat transfer coefficient and S represents saturation. The subscripts g, w and e represents gas, water and formation respectively.

When the fluid and reservoir properties are available, equation (22) can be used to get an estimate of the temperature at the sand-face. For the model well section, sand-face temperature was calculated at each payzone sequentially at a step of 10 feet moving upwards. Following graph shows the estimated sand-face temperatures in each payzone.

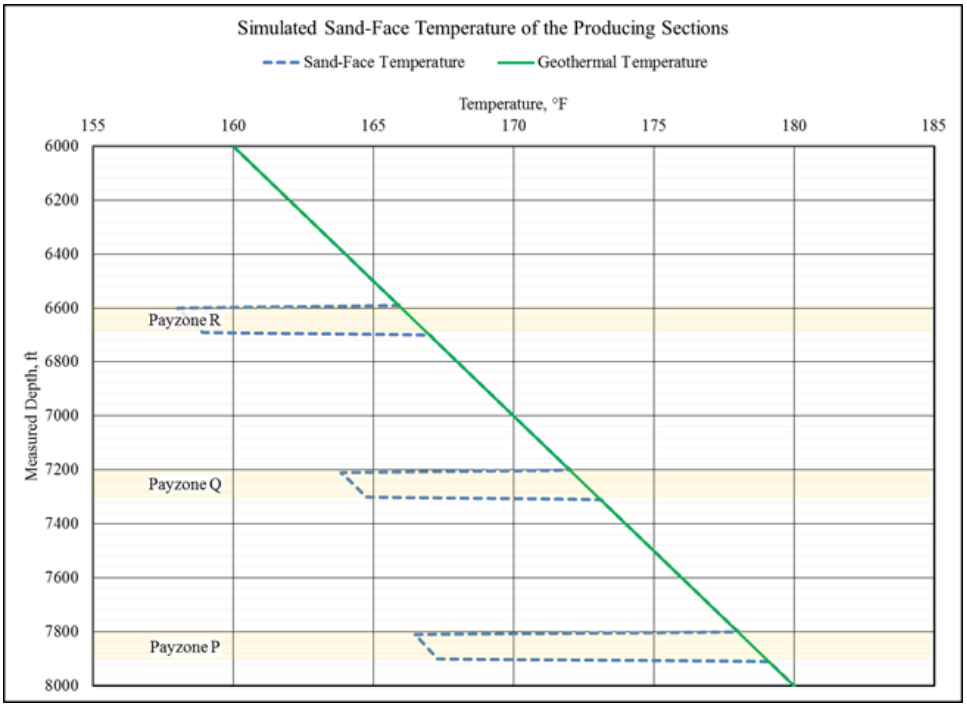

Figure 5: Generated synthetic sand-face temperature profile

Equation (26) requires the value of permeability for each of the payzones. To estimate permeability, following equation of gas flow rate was utilized,

$$q\left(\frac{Mscf}{d}\right) = \frac{kh\left[m(p_i) - m(p_{wf})\right]}{1638T}\left[logt + \log\frac{k}{\varphi(\mu c_t)_i r_w^2} - 3.23\right]^{-1} \quad \ldots\ldots\ldots (28)$$

Table 3: Estimated average payzone permeability

Payzone	Depth (ft)	Average Payzone Permeability (mD)
P	7800-7900	6
Q	7200-7300	15
R	6590-6690	5

3.2.2.3. Temperature Profile Data Generation in Producing Sections

A producing zone at the bottom of the wellbore has fluid coming in only from the reservoir. So, the estimated fluid temperature at that point is equal to the sand-face temperature. But, for rest of the producing sections above that have fluid coming in from the non-producing section just below it mixes with the fluid that is coming in from the reservoir at that section. As per assumptions made in subchapter 2.1, the mixing takes place instantaneuously and reaches thermal equilibrium before leaving the section. Additionally, no heat exchange takes place with the formation in this producing section and the fluid compositions are same for both fluids. For such assumptions, same energy balance for the developed model in sub-chapter 2.2 is valid. So, equation (13) can be rewritten in the following form,

$$T_{ni} = \frac{q_{n(i+1)}}{q_{ni}}\left[T_{n(i+1)} + C_{JT}\left(P_{ni} - P_{n(i+1)}\right) - \frac{g\Delta z sin\alpha}{C_P J g_c}\right] + \frac{q_{ni} - q_{n(i+1)}}{q_{ni}}\left[T_{r(i+1),avg} + C_{JT}\left(P_{ni} - P_{r(i+1),avg}\right) - \frac{1}{2}\frac{g\Delta z sin\alpha}{C_P J g_c}\right] \dots\dots\dots (29)$$

The temperature just below the producing section is known from the generated temperature profile from the method discussed in subchapter 3.2.2.1 and it can be considered $T_{n(i+1)}$ in this equation. The sand-face temperature at this producing section can be estimated using the methods discussed in sub-chapter 3.2.2.2. The average sand-face temperature of the incoming fluid is considered to be $T_{r(i+1),avg}$ and it is considered that the all the fluid volume is entering the wellbore at the average depth of the producing section for to simplify calculation steps. Rest of the variables are either assumed while

defining the model well or calculated. Thus, the temperature just above the producing section, T_{ni} from equation (28) can be calculated.

3.2.2.4. Generated Temperature Profile

As temperature data just above and below the producing section is generated, a straight line interpolation is done to get the temperature in points within the section. It is simplifying assumption for easy calculation of the profile over the short length of producing section. Attaching this profile with the temperature profile generated over the non-producing sections using the method discussed in sub-chapter 3.2.2.1, temperature profile for the model well section for assumed flowing conditions can be generated.

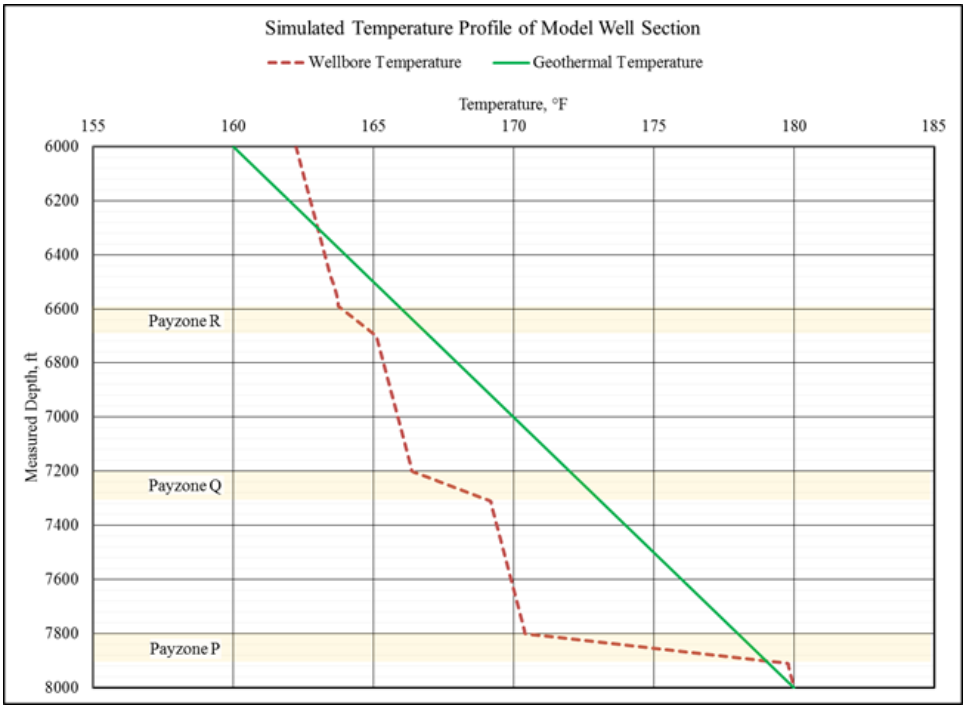

Figure 6: Generated synthetic temperature profile for the model wellbore section

3.3. Flow Profile from Model Using the Generated Synthetic Dataset

As discussed in sub-section 2.3, equation (13) can be utilized to estimate flow rate from each pay zone using the generated synthetic dataset in chapter 3. From the generated synthetic dataset, the temperature and pressure profile of the well section under investigation is known. The flow rate from each is unknown at this point. But, as the equation (13) requires an average sand-face temperature of each zone, it will be estimated from the procedure discussed in subchapter 3.2 using equation (22) repeated below,

$$T(r,t) = T_{ei} + \frac{C}{2B} e^{\frac{Dr^2}{2B}} Ei\left[-\frac{D(Ar^2+2Bt)}{2AB}\right] - \frac{C}{2B} e^{\frac{Dr^2}{2B}} Ei\left[-\frac{Dr^2}{2B}\right] \quad \ldots\ldots\ldots (22)$$

In equation (22), variables A, C and D require flow rate from the zone into the wellbore as an input parameter. But, that flow rate is the term that is being estimated through the use of the model developed in this study. So, an iterative method is developed to reach a simultaneous solution of flow rate and sand-face temperature. Steps of this iterative method is discussed below,

1. To begin, a reasonable assumption is made for flow rate from the shallowest perforation.
2. Using that assumed flow rate, the average sand-face temperature is calculated for that zone using equation (22).
3. Calculated average sand-face temperature is used to estimate zonal flow rate using the developed model.

4. If the calculated flow rate is higher than the assumed flow rate, assumed flow rate is increased by {(calculated flow rate-assumed flow rate)/2}. If the calculated flow rate is lower than the assumed flow rate, assumed flow rate is decreased by {(assumed flow rate-calculated flow rate)/2}.
5. Step 2 to step 4 is repeated until the assumed flow rate is equal to calculated flow rate. This value is considered to be the flow rate from that zone.
6. Repeated step 1 to step 5 for next zones sequentially.

Figure (7) shows the comparison of the actual flow profile we used to generate our synthetic dataset and the one calculated using the model.

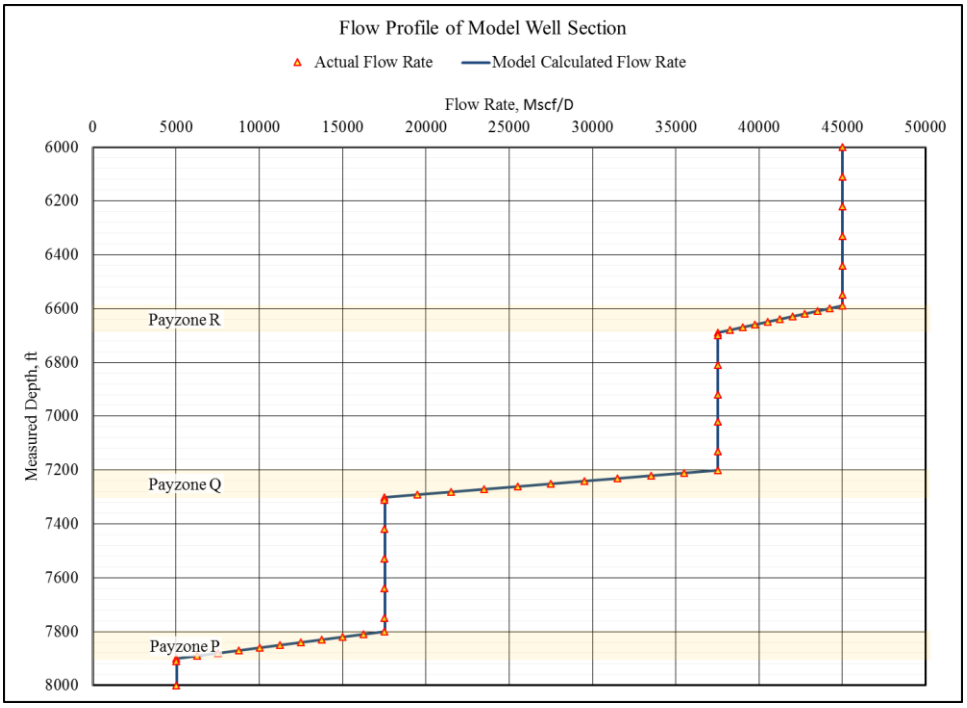

Figure 7: Estimated flow profile of the model wellbore section

3.4. Sensitivity Study

To study the sensitivity of the parameters in the model in estimating zonal flow contributions, we performed some analyses. Following subchapters will go through those analyses and discuss the effect of each individual parameter.

3.4.1. Effect Of Errors In A Single Variable

The first study is to investigate if changing a single individual parameter throughout the wellbore has a significant effect on the output flow profile. To do that, parameters are simply shifted in varying degrees, one at a time. This assesment gives a fair understanding of the signifacnce of each parameter in the model's output. Following subchapters discusses the results of this set of sensitivity studies for different parameters.

3.4.1.1. Effect Of Error In Wellbore Fluid Temperature

Wellbore fluid temperature, T_{ni} (°F) and $T_{n(i+1)}$ (°F) will be measured by DTS or temperature logging tool in field. These tools can have accuracy of ±0.01°F if modern sensors are in use. But, errors in fluid temperature measurement can still happen for different reasons. To replicate that uncertainty to some extent, an error of -1°F to +1°F in the value of wellbore temperature profile is considered throughout the model wellbore section. Figure (8) shows the effect of error in wellbore fluid temperature on the calculated zonal contributions.

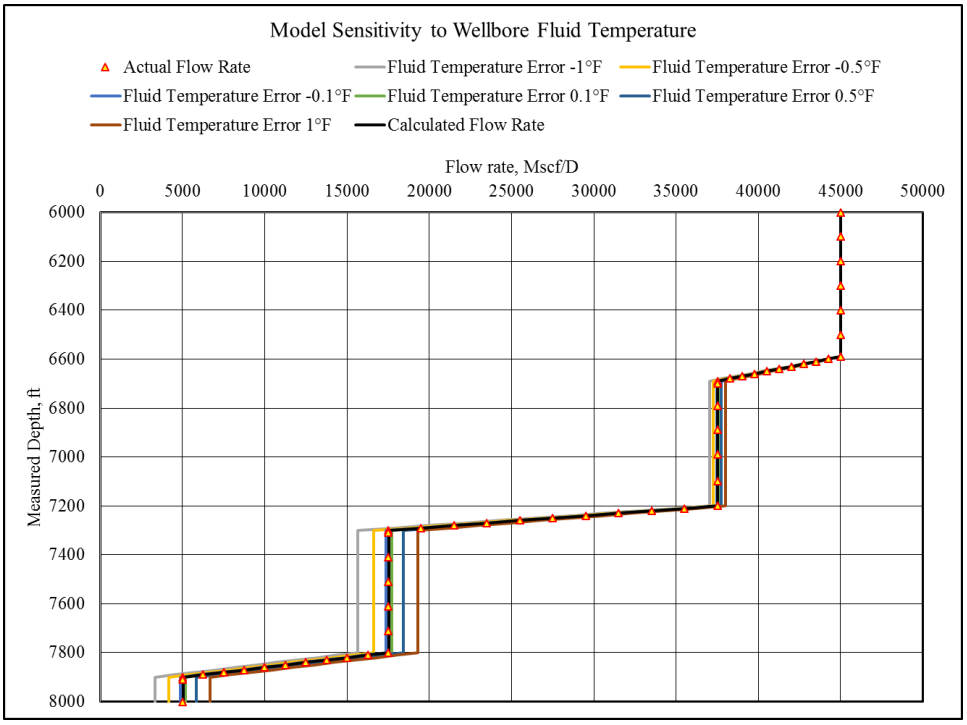

Figure 8: A sensitivity analysis of the estimated flow profile of the model well section for error in wellbore fluid temperature

From Figure (8), it can be noticed that very small errors in measurement or estimation of wellbore fluid temperature can lead to to very significant effect on the output flow profile. Table (4) shows the percentage error in flow rate estimate from each zone if errors to wellbore temperature values are introduced. Error of ±1°F in wellbore temperature profile of synthetic dataset can lead to ±6.8% error in estimated zonal flow rates. Error in output of the model can be higher in zones with smaller production rate as small change in temperatures across that zone can be hard to detect.

Table 4: Errors in zonal flow rate estimation for errors in wellbore fluid temperature

Zone	Fluid Temp Error -1°F	Fluid Temp Error -0.5°F	Fluid Temp Error -0.1°F	Fluid Temp Error 0.1°F	Fluid Temp Error 0.5°F	Fluid Temp Error 1°F
R	6.28%	2.96%	0.37%	-0.92%	-3.43%	-6.53%
Q	6.79%	3.31%	0.58%	-0.76%	-3.41%	-6.65%
P	-1.31%	-0.57%	-0.07%	0.17%	0.59%	1.06%

In summary, this analysis demonstrates that having an accurate estimation or measurement of wellbore fluid temperature is of utmost importance for this model to work for actual field cases.

3.4.1.2. Effect Of Error In Average Sand-Face Temperature Estimation

During synthetic data generation, average sand-face temperature, $T_{r(i+1),avg}$ (°F) for each of the payzones was calculated using the equation (22) discussed in subchapter 3.2. For this synthetic case, as all the reservoir properties are known, the said equation was used to calculate the average sand-face temperature. But, in field, estimation or measurement of sand-face temperature is the most challenging part of using this model. There are significant uncertaintys involved with sand-face temperature estimation using any accepted model if measurement is unavailable. To replicate that uncertainty to some extent, an error of -1°F to +1°F in the value of average sand-face temperature of the three

payzones is considered. Figure (9) shows the effect of error in average sand-face temperature on the calculated zonal contributions.

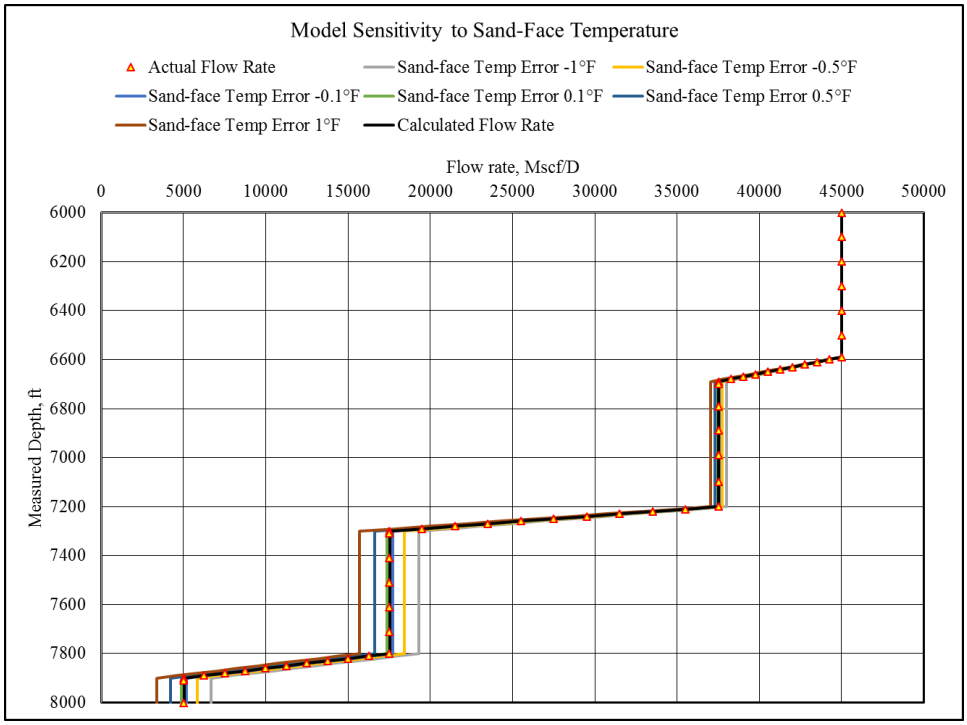

Figure 9: A sensitivity analysis of the estimated flow profile of the model well section for error in sand-face temperature

From Figure (9), it can be noticed that very small errors in measurement or estimation of average sand-face temperature of the pay zones can lead to to very significant effect on the output flow profile. Although, modern temperature sensors and optical fiber based DTS are really accurate and can measure temperature upto very fine resolution, the model leaves little room for error for sand-face temperature. It becomes more significant while we are using theoretical models to estimate sand-face temperature which will be discussed in details later in this subchapter and in the field case studies

explained in next chapter. Table (5) shows the percentage error in flow rate estimate from each zone if we introduced errors to average sand-face temperature values.

Table 5: Errors in zonal flow rate estimation for errors in sand-face temperature

Zone	Sand-face Temp Error -1°F	Sand-face Temp Error -0.5°F	Sand-face Temp Error -0.1°F	Sand-face Temp Error 0.1°F	Sand-face Temp Error 0.5°F	Sand-face Temp Error 1°F
R	-6.46%	-3.40%	-0.91%	0.35%	2.91%	6.18%
Q	-6.58%	-3.37%	-0.76%	0.57%	3.27%	6.68%
P	1.08%	0.60%	0.17%	-0.06%	-0.58%	-1.29%

In summary, this sensitivity analysis demonstrates that having an accurate estimation or measurement of sand-face temperature is of utmost importance for this model to work for actual field cases.

In this study, expression (22) is used to estimate the sand-face temperature for both synthetic dataset and field case studies. If the reservoir parameters are available, sand-face temperature values depend on our knowledge of geothermal temperature profile. So, knowing the effect of geothermal temperature assumption can be helpful going it field data application. For this test, the gradient 0.0115°F/ft is kept constant and shifted the line in either direction by a maximum of 1°F. Figure (10) shows the results of this investigation. For correct estimation of rest of reservoir properties, changes in only geothermal temperature profile has significant effect. For the generated synthetic dataset, error of ±1°F can cause ±6% error calculated zonal flow rates.

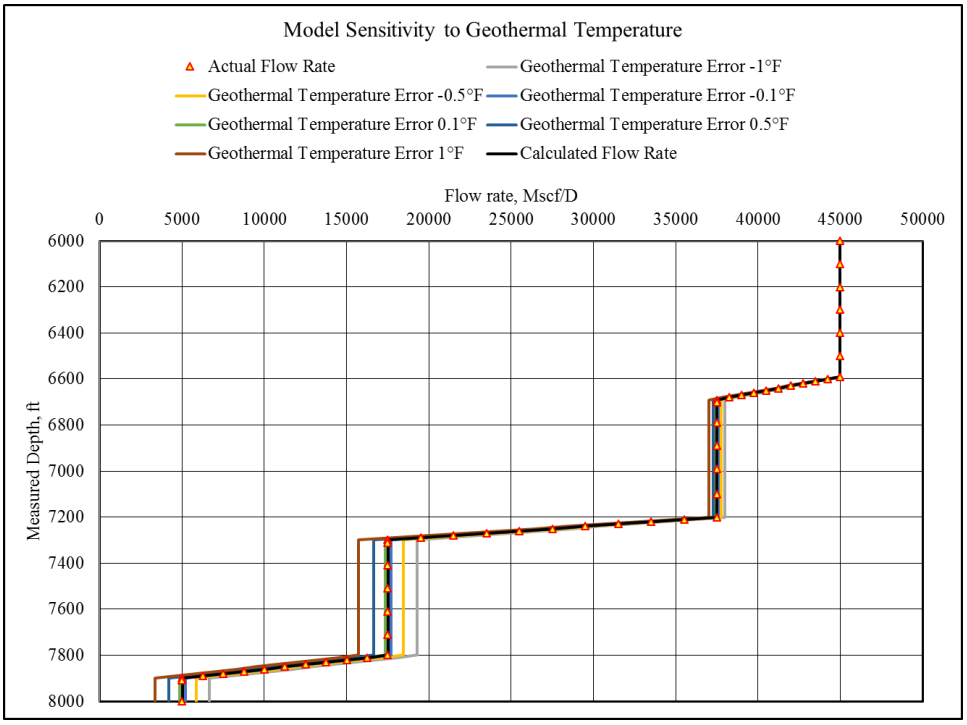

Figure 10: A sensitivity analysis of the estimated flow profile of the model well section for error in geothermal temperature

Similarly, expression (22) also requires the value of permeability. If geothermal gradient and other reservoir parameters like porosity etc. are available, sand-face temperature values depend on our assumption or estimates of reservoir permaebilities. Accurate estimation of permeability in such multi-zone completions can be difficult and can always have error in field cases. To simulate that, the permeabilities of the 3 zones were varied by upto ±10% and the resulting output of zonal flow rates from the model was observed. Figure (11) shows the results of this analysis where it can be concluded that erroneous permeability values can result in significant errors in zonal flow rate estimates

from the model. For the generated synthetic dataset, error of ±10% in permeability can cause ±6% error calculated zonal flow rates.

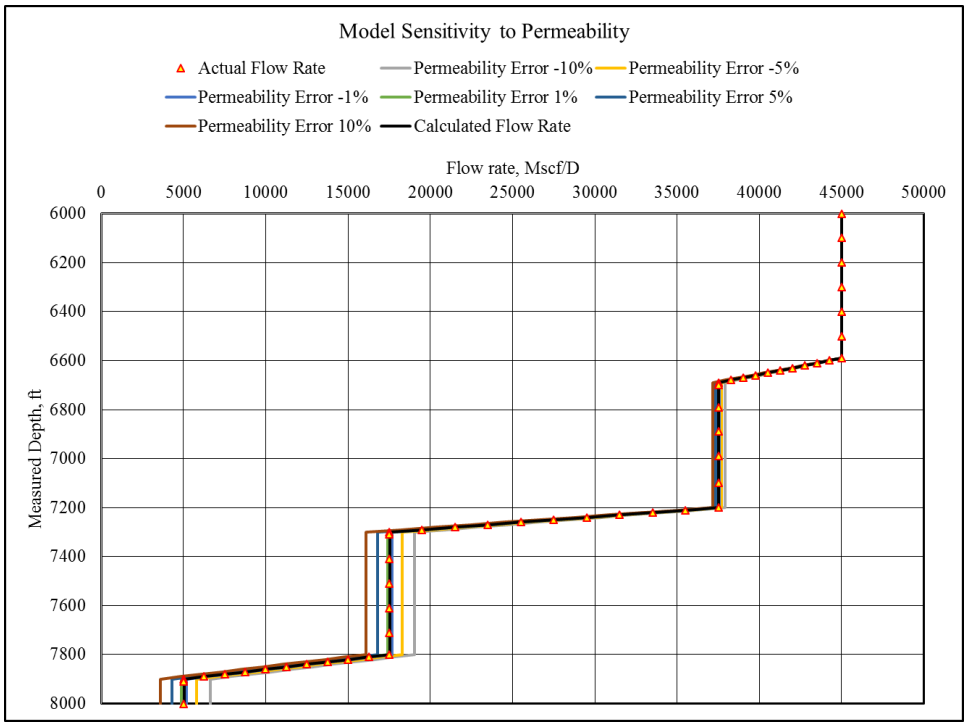

Figure 11: A sensitivity analysis of the estimated flow profile of the model well section for error in permeability

3.4.1.3. Effect Of Error In Pressure Profile Measurement

To utilize the model that we developed, we need wellbore pressure profile data which can be from optical fiber based DPS or pressure gauges set up at different depth or production logging runs. The accuracy and resolution of this pressure data will depend on and be limited to the specifications of the sensors and gaugues that is used. For our synthetic well section, we calculated the pressure profile from industry accepted published method discussed in sub-chpater 3.2. But, we can introduce some errors to that calculation

to replicate measurement errors in the field. Six cases were considered for this test where we introduced error to the pressure profile data which ranges from -10% to +10%. Figure (12) illustrates the effect these errors in pressure profile have on the calculated zonal contributions.

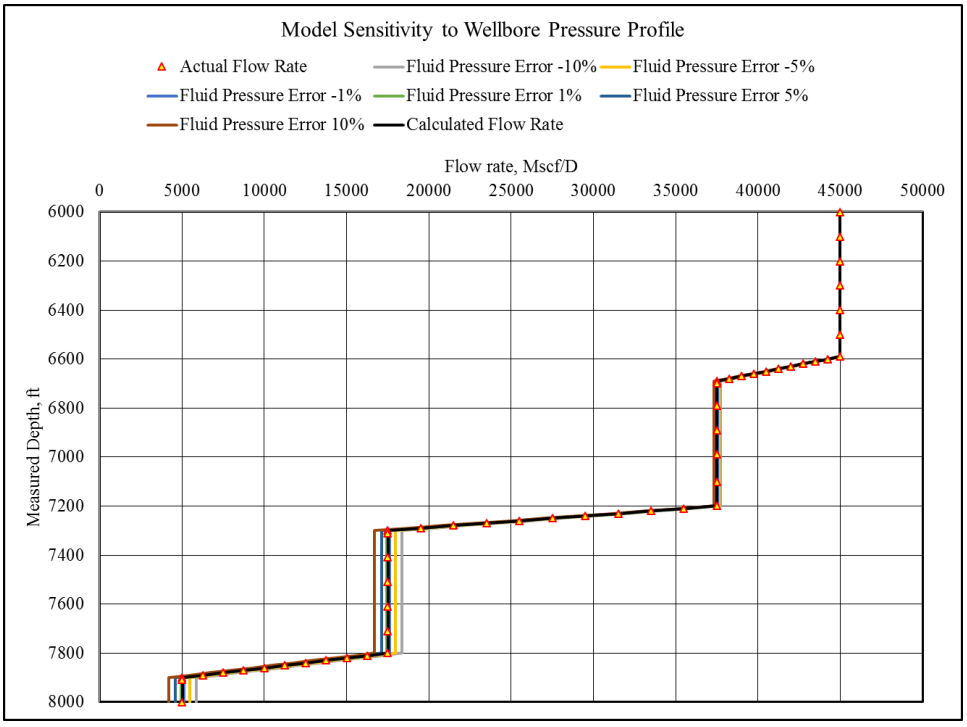

Figure 12: A sensitivity analysis of the estimated flow profile of the model well section for error in wellbore pressure profile

It can be observed from Figure (12) that for small errors in measurement of pressure profile induces acceptable error ranges in output flow profile. Even with 10% errors in pressure data, we get a maximum of around 3% error in output zonal flow rate estimates from our model. Table (6) displays the percentage error in flow rate estimate in each zone for the errors we added to the pressure profile for our model validation.

Table 6: Errors in zonal flow rate estimation for errors in wellbore pressure

Zone	Pressure (psi) Error -10%	Pressure (psi) Error -5%	Pressure (psi) Error -1%	Pressure (psi) Error 1%	Pressure (psi) Error 5%	Pressure (psi) Error 10%
R	-3.01%	-1.65%	-0.56%	-0.01%	1.10%	2.48%
Q	-3.13%	-1.62%	-0.40%	0.21%	1.45%	3.00%
P	-0.25%	-0.07%	0.04%	0.07%	0.14%	0.17%

1% error in pressure profile might seem significant at first glance, but in a typical well, pressure in the interest zone can be anywhere from 1000 psi to very high pressure. In those cases, 1% error means at least 10 psi error. Most modern pressure sensors and gauges are far more accurate than that and has finer resolution. So, it is not difficult to stay within 1% range. Also, from surface flow rates can easily give us estimates of pressure of a point just above the topmost perforation, especially for gas wells. With a rough expected estimation of zonal flow contribution, we can estimate the pressure profile which can be with ±10% range of actual pressure profile. So, we can see that even with that big error range in pressure profile (eg, ±200 psi error in a point where bottomhole flowing pressure is 2000 psi), we can still get a good enough estimation of zonal flow allocation. This can be an opportunity to investigate the option of using only temperature measurements to estimate zonal flow contribution from our model and use estimates of pressure at different points in the wellbore .

3.4.1.4. Effect Of Errors In Specific Heat Capacity

Heat Capacity of the fluid, Cp (Btu/lbm.°F) was considered to be constant for our data generation and consequent flow profile estimation. To check it's sensitivity on the zonal contribution profile, we decided to add errors from -10% to +10% in heat capcity value throughout the wellbore section in the model even though the dataset that was generated using 0.5 Btu/lbm.°F. That means we used heat capacity value from a minimum of 0.45 Btu/lbm.°F to a maximum of 0.55 Btu/lbm.°F to estimate zonal flow contributions. Figure (13) shows a graph which displays the effect of this significant change in heat capacity value on the calculated zonal contributions. The graph clearly demonstrates that even with shift in the heat capacity curve, the output values and flow profile looks very similar for the 6 cases we tried. This check proves that as long as we have consistency in the value of Cp is close to the actual Cp, the flow profile remains similar. So, it is important to have a good idea about the value of Cp. Table (7) shows the percentage error in flow rate estimates in each zone.

Table 7: Errors in zonal flow rate estimation for errors in specific heat capacity

Zone	Cp (Btu/lbm-°F) Error -10%	Cp (Btu/lbm-°F) Error -5%	Cp (Btu/lbm-°F) Error -1%	Cp (Btu/lbm-°F) Error 1%	Cp (Btu/lbm-°F) Error 5%	Cp (Btu/lbm-°F) Error 10%
R	-5.57%	-2.87%	-0.80%	0.23%	2.23%	4.67%
Q	-5.13%	-2.58%	-0.58%	0.40%	2.34%	4.71%
P	-0.29%	-0.05%	0.04%	0.06%	0.03%	-0.11%

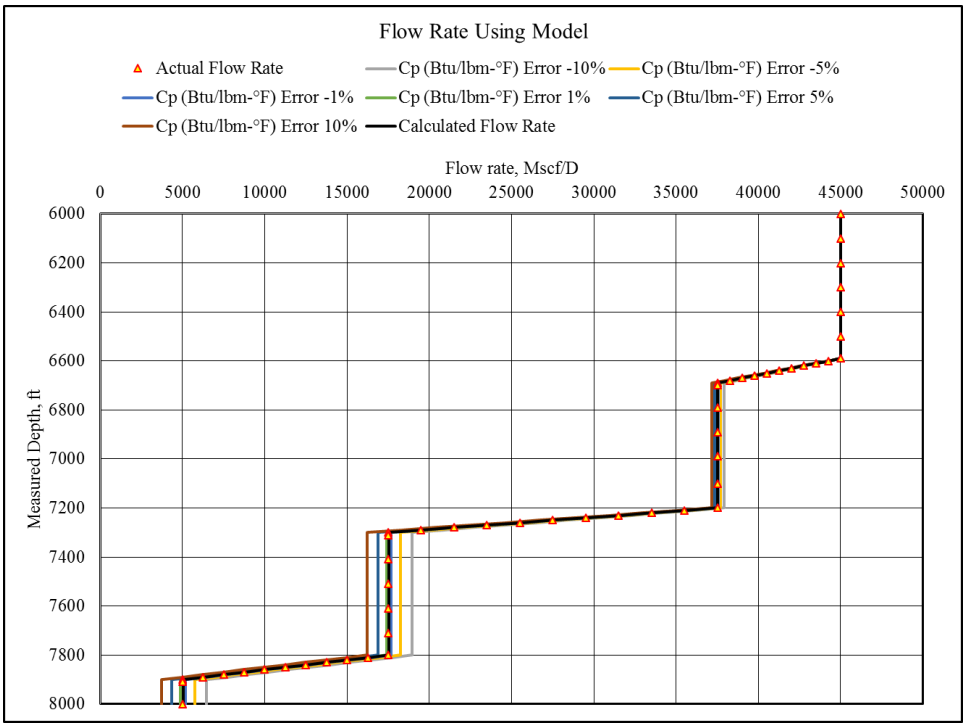

Figure 13: A sensitivity analysis of the estimated flow profile of the model well section for error in specific heat capacity

3.4.2. Effect Of Errors In Multiple Variables

In this subchapter, we will discuss the results of the sensitivity study where multiple variables were varied simultaneously. To perform such a study, we used Monte-Carlo method of statistical analysis, which is a computational algorthim where repeated random sampling is performed for each of the variables for a large number of iterations to obtain a distribution of results. Such an analysis allows us to have random error introduced to each of the variables in each different iterations which are completely unrelated and check the impact of each variables on the final output of the model. For this study, we used excel add-in from Palisade Software's The DecisionTools Suite.

Following table shows the minimum and maximum errors introduced in the values of each variables. We assumed that these errors follow a triangular distribution with 0 or 0% as the means of the input distributions.

Table 8: Assumed variability of the parameters in the required for the developed model

Paramter Name	Minimum	Maximam
Specific Heat Capacity (Btu/lbm.°F)	-10%	+10%
Wellbore Pressure (psia)	-10%	+10%
Wellbore Fluid Temperature (°F)	-1	1
Average Sand-face Temperature (°F)	-1	1

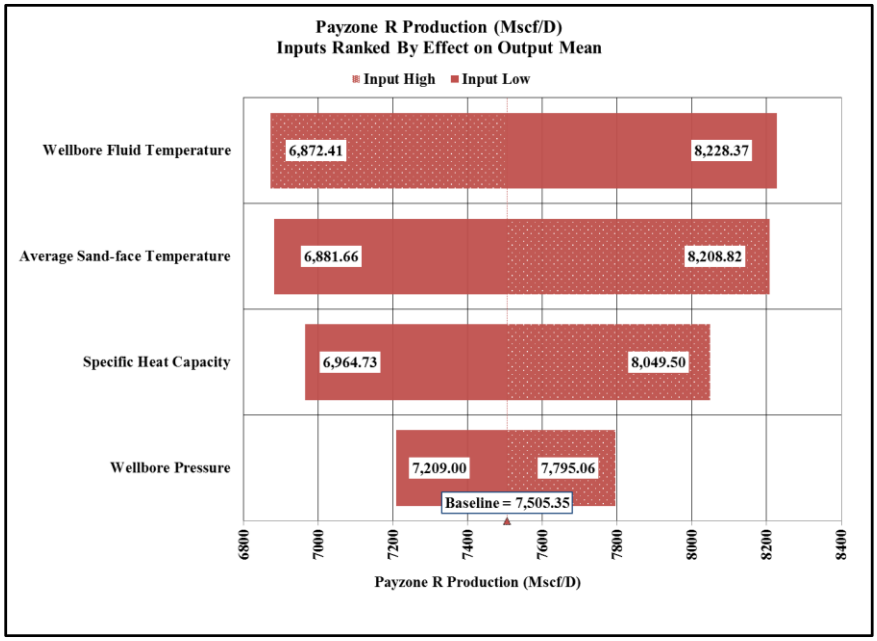

Figure 14: Tornado chart showing effects of variables on model estimated flow rate from payzone R

After running the simulation for 1,000 iterations, we get a distribution of values for Flow rates form different zones. From the analysis we see that wellbore fluid temperature and sand-face temperature has the largest effect on the output of the model for Payzone R, the shallowest zone. Another observation that can be made from the tornado chart in figure (14) and figure (15) for this zone is that, the effects of wellbore fluid temperature and sand-face temperature has opposite influence on zonal flow contribution. We also notice from figure (14) and figure (15) is that wellbore pressure profile has lowest impact among the variables in study and minimal influence on the variance of the output flow rate of that zone.

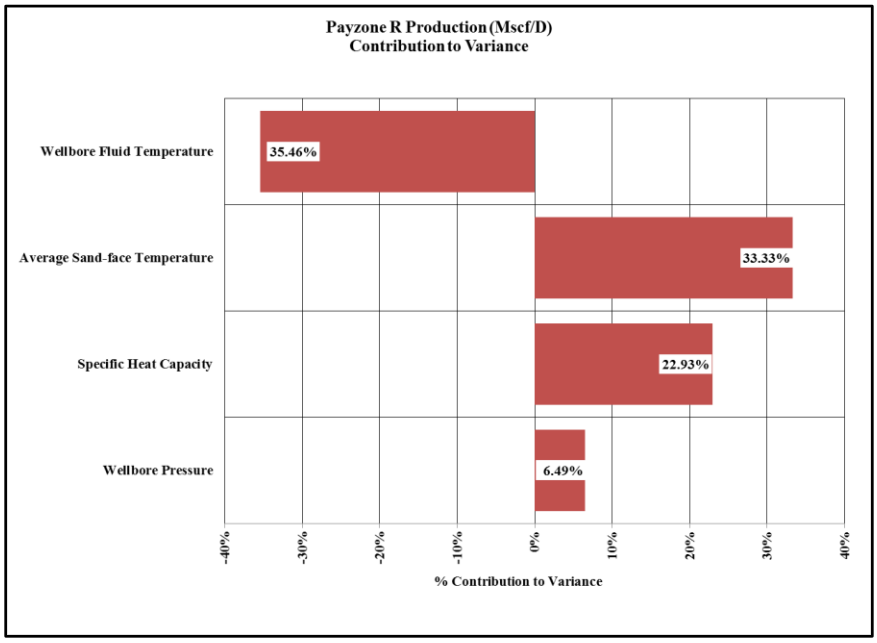

Figure 15: Tornado chart showing contributions to variance of model estimated flow rate from payzone R

The simulation also shows a detailed spider chart showing the change in the output flow rate for the variation in different variables. Figure (16) shows that spider chart. This

chart helps us visualize that with increasing pritive errors of wellbore fluid temperature, the output flow rate decreases. While for rest of the variables, output flow rate increases with increasing positive errors.

For payzone Q, we have a different scenario as the model output of payzone Q depends on the model output flow rate of Payzone R. So, we performed another set of 1,000 iterations to check the effect of variables in the output of Payzone Q. Figure (17) and Figure (18) shows the tornado charts for the analysis done for payzone Q.

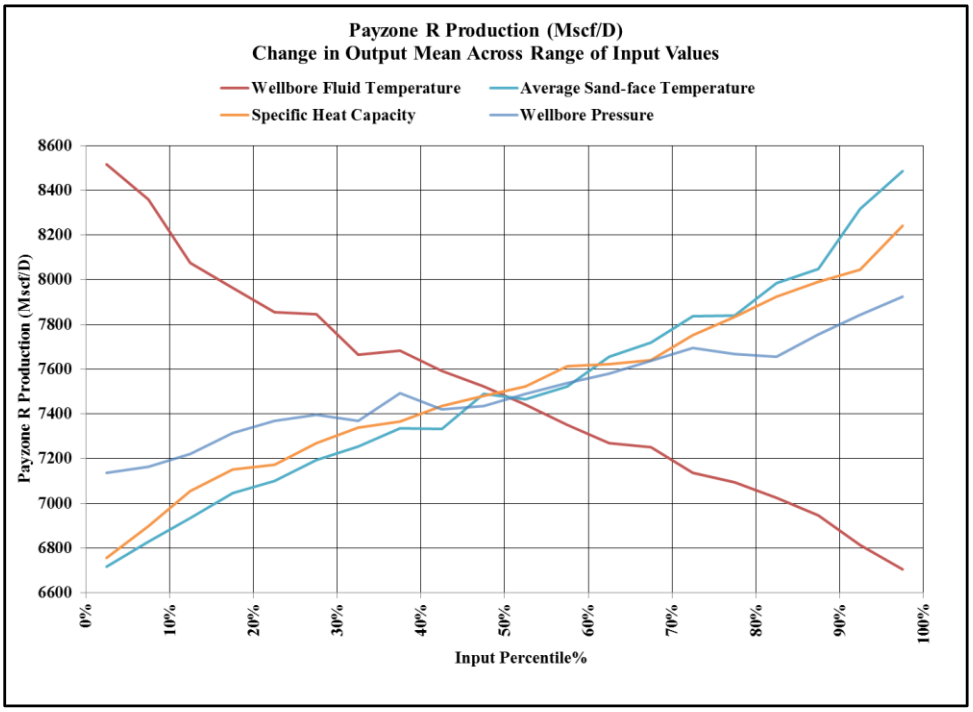

Figure 16: Spider chart for model estimated flow rate from payzone R

We can observe from the tornado charts that the influence of different variables are similar to the case of Payzone R. But, Payzone R production influences the mean of the output flow rate from payzone Q to some extent. But, variance of the model output

flow rate from payzone Q does not get effect significantly by the uncertainty of the flow rate from shallower zone above it.

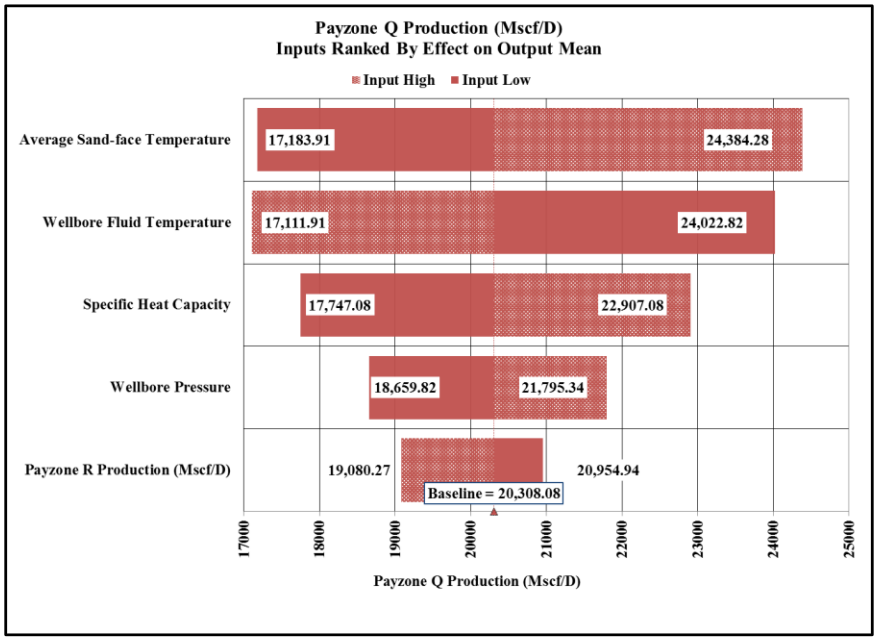

Figure 17: Tornado chart showing effects of variables on model estimated flow rate from payzone Q

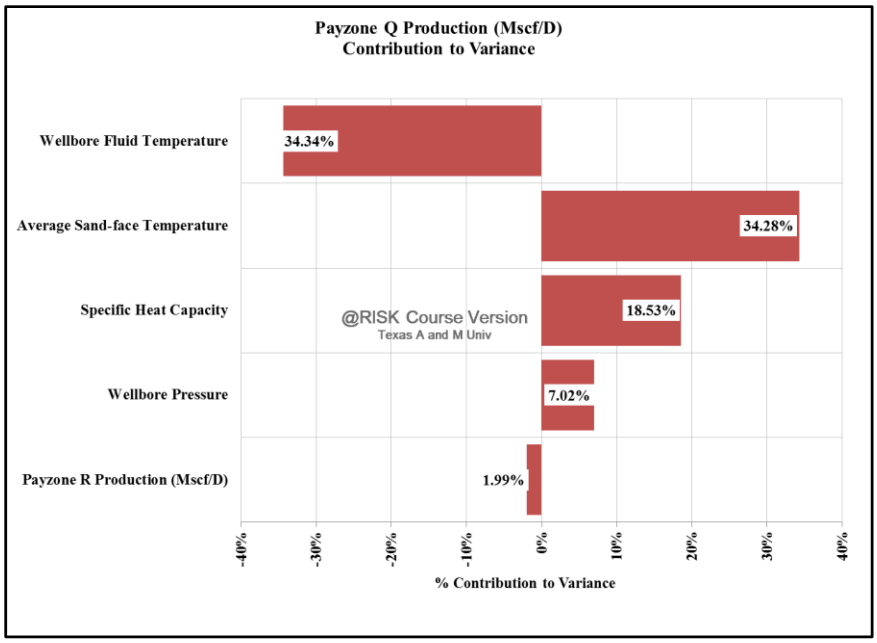

Figure 18: Tornado chart showing contributions to variance of model estimated flow rate from payzone Q

4. FIELD CASE STUDIES

The zonal flow allocation model developed in chapter 2 can be used for any kind of fluid if all the properties are known. But, it was developed having a vertical or near vertical conventional gas well in mind. To investigate utilization of this model in actual gas wells, we collected relevant well data from PetroBangla in Bangladesh. In following subchapters, application of the model in such wells will be discussed.

For this study, we have production logging raw data for 3 dry gas wells from a large dry gas field and we have access to 3 different surface flow rate cases for each of those well. The reservoirs in this field are predominantly stratified sandstone with shale formations forming impermeable layers in between two reservoirs. These 3 wells are atleast a few miles apart from each other although in the same field and are drilled vertically or in S-type design. In all the cases, the section of interest in the well is close to being vertical and does not have much deviation change. The wells are completed with traditional perforated completions. As the wells are not equipped to measure temperature and pressure in real time with DTS and DPS, we only have access to temperature and pressure data from production logging run performed during periodic well surveillance. The data used in this chapter are from the surveillance program performed in 2013 and 2014. Spinner logging was also performed as part of the production logging suite, which gives us a flow profile of the wells if interpreted. This interpreted flow profiles are used in the following subchapters to validate the model developed in chapter 2. Estimated

porosity of each reservoirs were provided by the operator based on open hole log interpretation.

4.1. Data Preparation for Model Validation

Validating the model required temperature, pressure and flow profile for 3 different surface flow rate cases for each of the 3 wells. To interpret raw production logging data (Spinner data) to get flow profile data and the temperature and pressure profile associated with it, a commercial production logging interpretation software, Kappa Emeraude v2.60.12 was used.

Kappa Emeraude takes raw data from production logging as input, usually in .las format and allows the user to interpret that dataset. In this study, production logging data for aforementioned 9 cases were interpreted. Separate individual spinner calibration was done for each of the cases in multiple stations in the well. The stations for calibration was chosen in a way that each of the producing and non-producing sections have atleast one station.

The zonal flow allocation model discussed in this study requires the average sand-face temperature of the incoming fluid at each zone. The wells in this study was not equipped with sand-face temperature measurement sensors or completeion that allows the use of such sensors. So, to have an estimate of incoming fluid temperature, equation (22) discussed in subchapter 3.2 was used. We assumed a fixed geothermal gradient of 0.0115 °F/ft and assumed that the ground temperature in the surface is 58°F. The expression in

equation (22) requires values of variables A, B, C & D. Three of these four variables involves the flow rate from that zone. As we do not have any better source for sand-face temperature for our case studies, we performed the iterative method for simultaneous solution of zonal flow rate and sand-face temperature as discussed in subchapter 3.3.

To get a value of variable C in equation (22) requires the value of permeability of that reservoir. We utilized the following equation of transient natural gas flow rate for any zone for 2 of the higher surface flow rates for each well.

$$q\left(\frac{Mscf}{d}\right) = \frac{kh\left[m(p_i) - m(p_{wf})\right]}{1638T}\left[logt + \log\frac{k}{\varphi(\mu c_t)_i r_w^2} - 3.23\right]^{-1} \quad \ldots\ldots\ldots (28)$$

Thus we end up with two equations for each of the cases for any zone in any of the well. By solving those equation pairs, we end up with approximate permeability of the reservoirs.

In calculation of all the variables in equation (22) for all zones in the 3 wells, following input parameters were kept constant.

Table 9: Input parameters for all 3 field case studies

Input Parameter	Value	Unit
Gas Specific Gravity, γ_g	0.6	
Formation Density, ρ_{form}	165.43	lb/ft^3
Formation Specific Heat, $c_{p\text{-}form}$	0.2	$Btu/lb.$°F
Reservoir Radius, r_e	4000	ft
Heat Transfer Coefficient, h_c	1	$Btu/hr - ft$^2°F
Geothermal Gradient	0.0115	°F/ft
Production time, t	1	days

4.2. Field Case Study – Well A

Well A is S-Type well with maximum deviation angle being 38.44° and terminal deviation angle is 19.47°. This well is plugged at measured depth of 12,749 ft or true vertical depth of 11,115 ft. There is a fish in this well that does not allow production logging tools to reach beyond 12,470 ft. The production casing of this well has an internal diameter of 4.778 inch and it runs from surface to total depth of this well.

Following table shows the perforation that are currently existing in the wellbore. The average porosity values in table are interpreted by the operator and provided to us. The average permeability and average reservoir pressure of the zones are estimated using the method discussed in subchapter 4.1 using equation (28).

Table 10: Well A perforations

Perforation	From (ft)	To (ft)	Average Porosity	Estimated Average Permeability (mD)	Estimated Average Reservoir Pressure (psia)
Perforation 7	11,709.6	11,775.2	0.173	27.5	2,075
Perforation 6	11,814.56	11,935.92	0.173	-	-
Perforation 5	11,965.44	12,063.84	0.18	6.5	2,130
Perforation 4	12,129.44	12,201.6	0.175	5.9	2,573
Perforation 3	12,270.48	12,404.96	0.175	9.7	2,199
Perforation 2	12,444.32	12,542.72	0.175	-	-
Perforation 1	12,608.32	12,706.72	0.179	-	-

Perforation 1 and Perforation 2 are below the accessible depth of 12,470 ft. So, data from those zones are not available. However, measurements just below Perforation 3

is known. So, we take the flow rate just below Perforation 3 and estimate contributions from the perforations above that point.

For this well, we have access to data from production logging performed in 3 different surface flow rate which are 39.1 MMscf/D, 30.9 MMscf/D and 23.5 MMscf/D. In this study, we consider that only surface flow rate was changed for each case and rest of the external influncers were kept constant.

Following 3 figures show the spinner calibration graph for the 3 cases. The highlighted points and the highlighted regression line is for calibration zone 1. Slope and intercept values are presented in the appendix C.

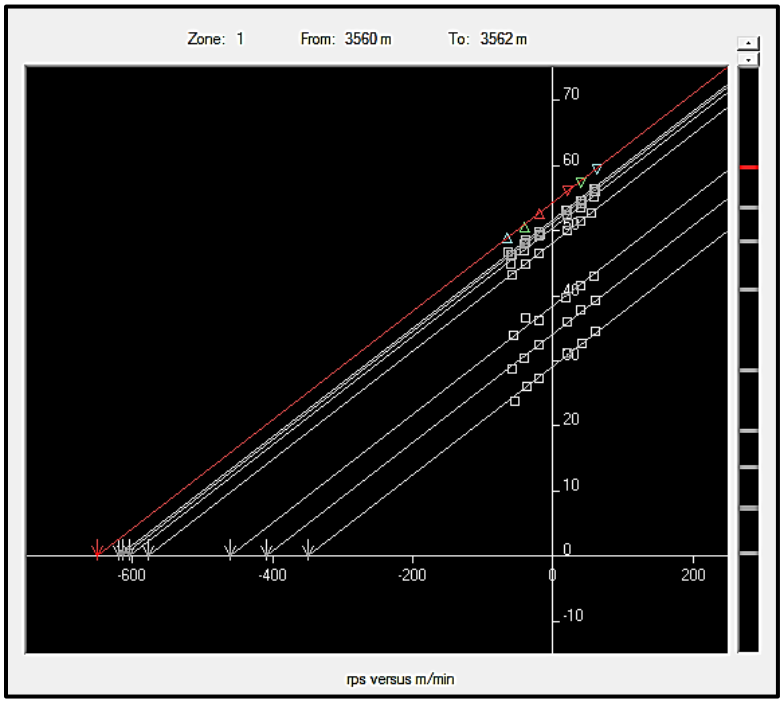

Figure 19: Spinner calibration for Well A 39.1 MMscf/D case

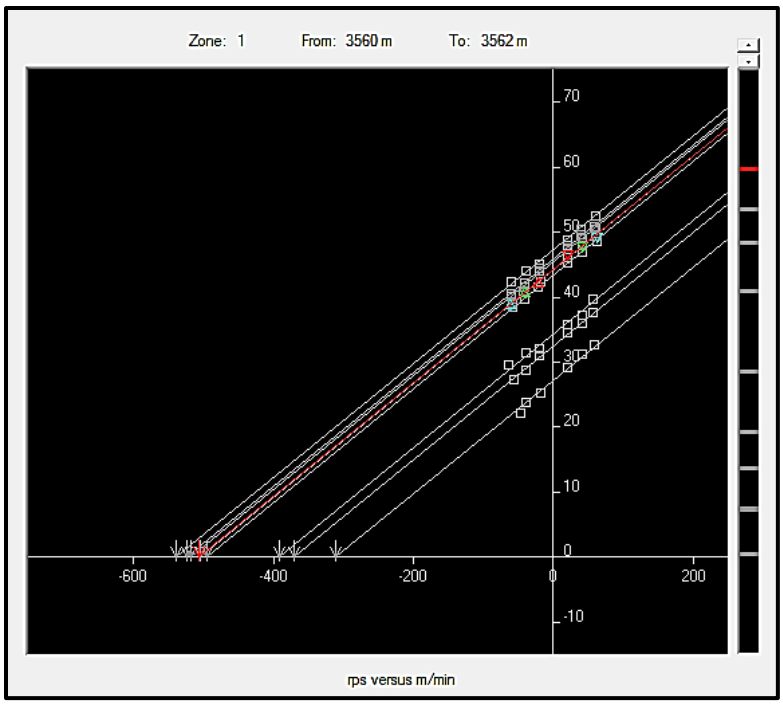

Figure 20: Spinner calibration for Well A 30.9 MMscf/D case

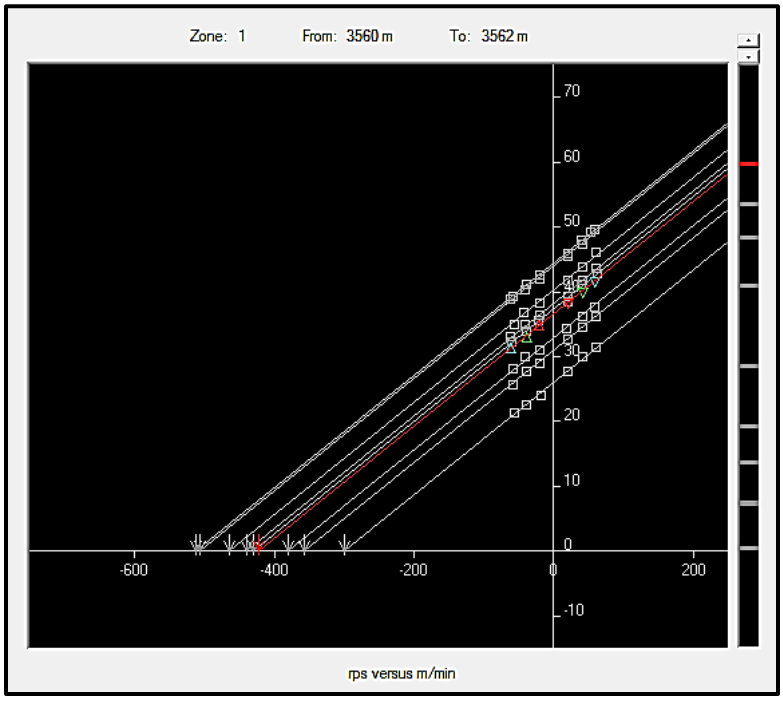

Figure 21: Spinner calibration for Well A 23.5 MMscf/D case

Following figure show the temperature profiles of the Well A section under investigation while the surface production rate is 39.1 MMscf/D, 30.1 MMscf/D and 23.5 MMscf/D.

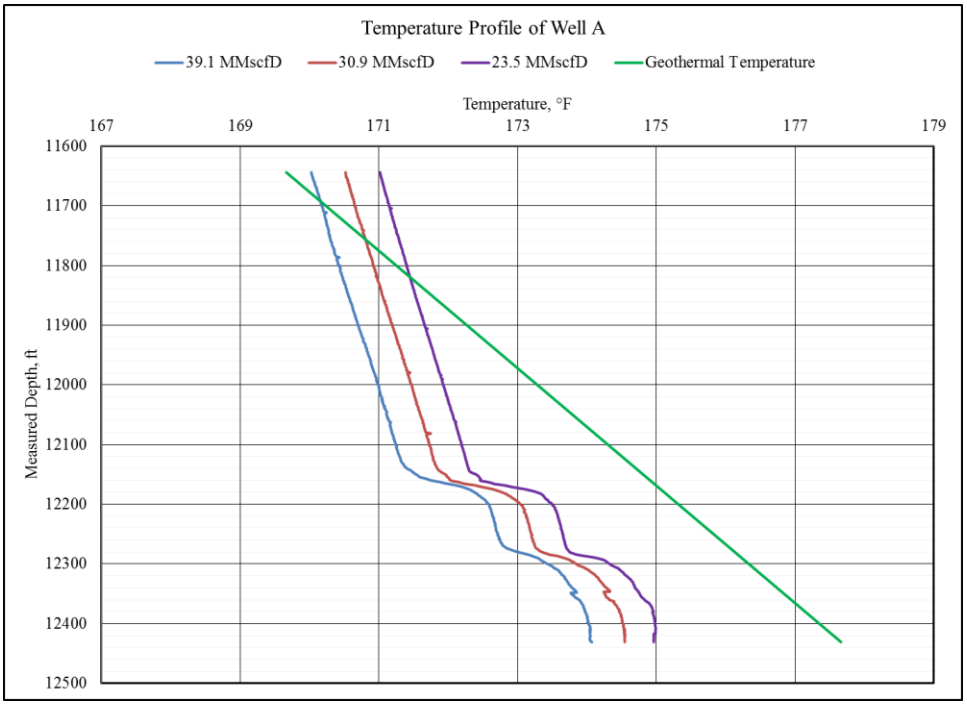

Figure 22: Temperature profile of Well A

One observation that can be made in Figure (22) is that wellbore temperature for all 3 cases follow similar shape. But, The wellbore fluid temperature for 39.1 MMscf/D case is a bit cooler than the 30.1 MMscf/D case which is subsequently cooler compared to the wellbore fluid temperature in 23.5 MMscf/D case. This is typical for gas wells when the reservoir pressure is not too high. In such scenarios, gas cools down as it expands due to Joule-Thompson cooling effect. For larger pressure drop, we see larger temperature drop when the gas enters the wellbore. As in 39.1 MMscf/D case, the surface flow rate is

higher, we can safely conclude that the zonal flow rate is higher than the 30.9 MMscf/D case and 23.5 MMscf/D case. Higher flow rate corresponds to larger pressure drop from reservoir to the wellbore for the same reservoir which results cooler fluid entering the wellbore. Thus, the temperature profile for 39.1 MMscf/D case is comparatively colder than 30.9 MMscf/D case which is again colder than 23.5 MMscf/D case.

Figure (22) also helps us see that there are significant change in the wellbore fluid temperature in perforation 3 and perforation 4. Which gives us a qualitative idea that both of those perforations have significant production. Perforation 6 is a case of outflow from the wellbore to the reservoir (indicated by spinner flowmeter) which means it is a depleted zone and the downhole flowing pressure has to be decreased to lower value in order to produce from that zone. The model developed in this study is based on mixing cup approach which requires inflow from the reservoir into the wellbore, thus making the model invalid for perforation 6.

Another observation that can be inferred from the figure (22) is that change of fluid temperature across perforation 5 and perforation 7 due to incoming fluid of different temperature are negligible. This situation qualitatively tells us that the flow rate from these zones are small compared to other higher producing zone. The temperature profile almost follows the same trend above the depth of perforation 4 which makes it difficult to detect accurate flow rate from those zones.

Figure (23) shows the pressure profile of the wellbore section under investigation,

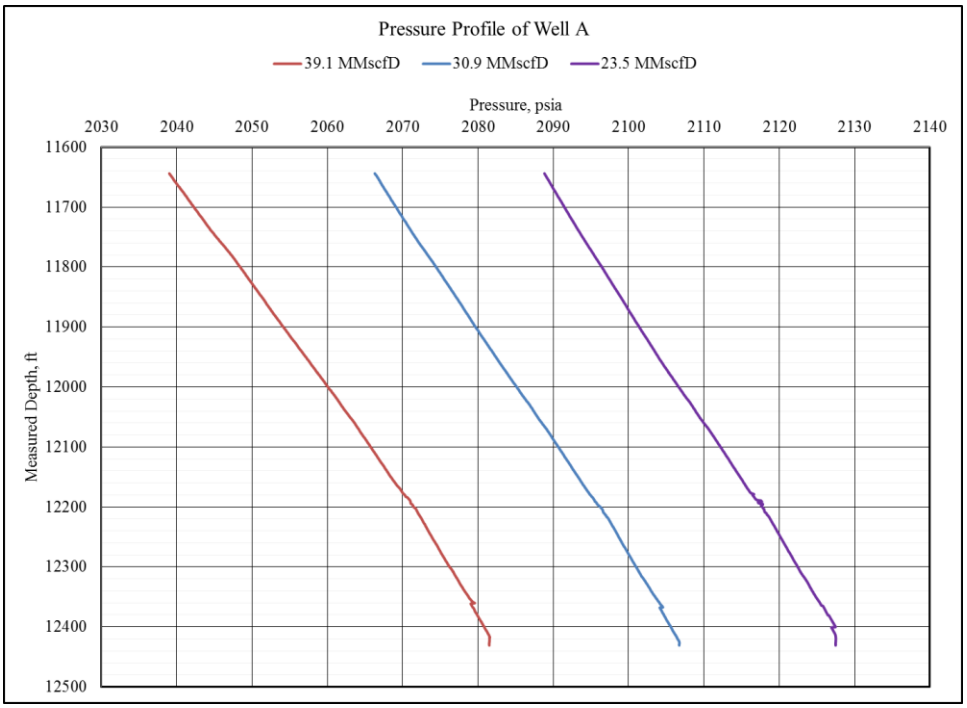

Figure 23: Pressure profile of Well A

Utilizing the the temperature profile and pressure profile shown above, we get the zonal flow allocation presented in figure (25), figure (26) and figure (27). Perforation 6 was ignored while estimating flow profile of as this zone has outflow towards the reservoir for all the cases. Also, perforation 5 and perforation 7 has outward flow for 23.5 MMscf/D case. So, we have attempted a different analysis by assuming that we know the value of outflow rate in different perforations and performed zonal flow allocation again with our model. The results of those attempts is presented in figure (28), figure (29) and figure (30).

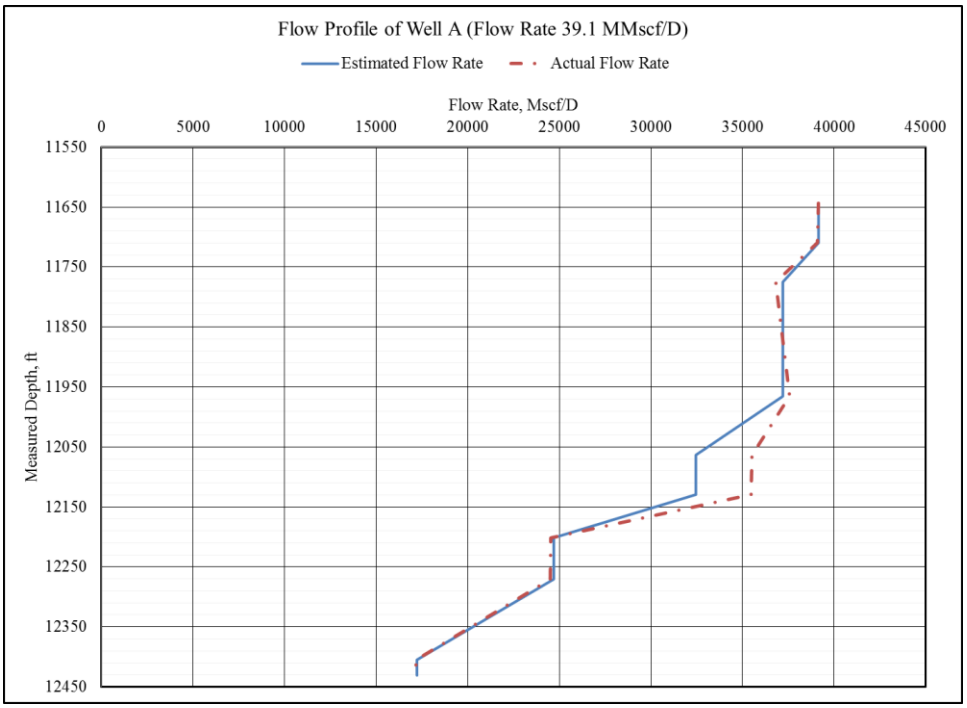

Figure 24: Estimated flow profile of Well A (39.1 MMscf/D case)

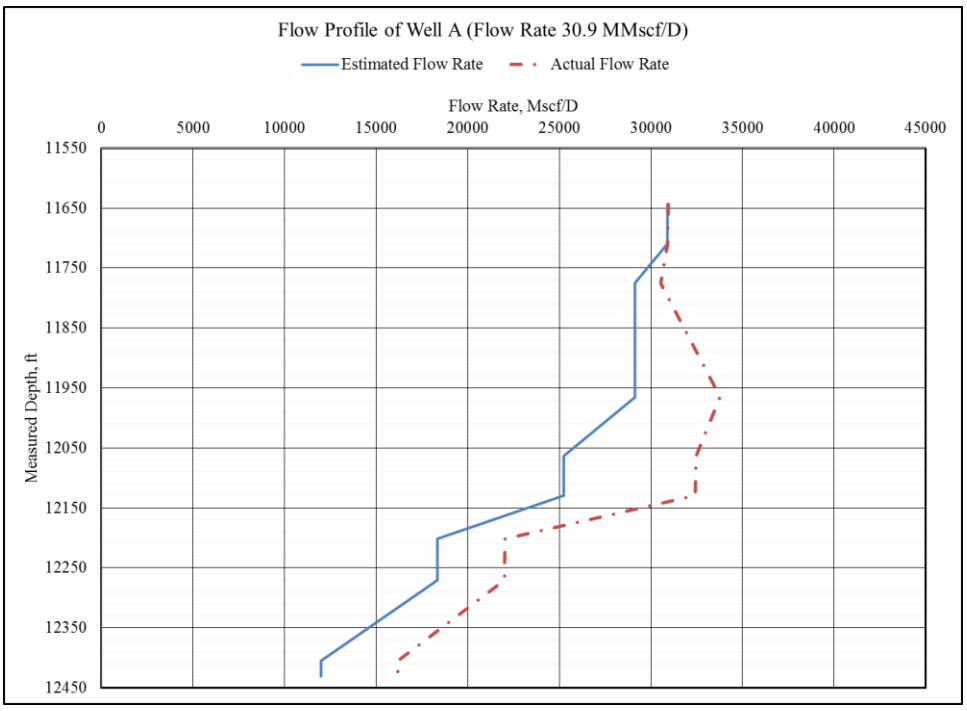

Figure 25: Estimated flow profile of Well A (30.9 MMscf/D case)

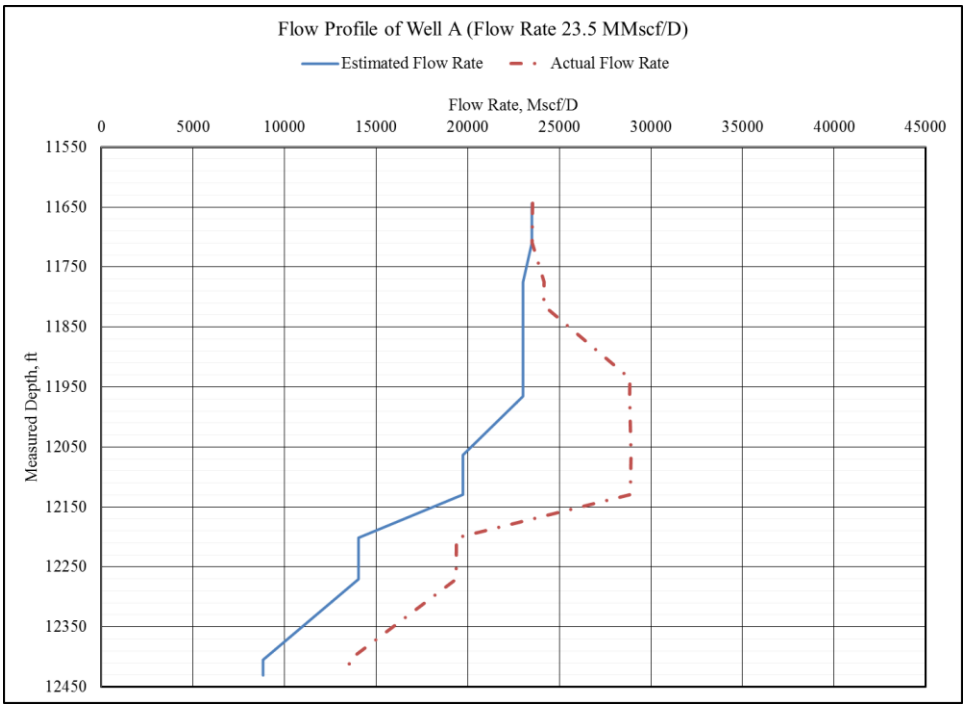

Figure 26: Estimated flow profile of Well A (23.5 MMscf/D case)

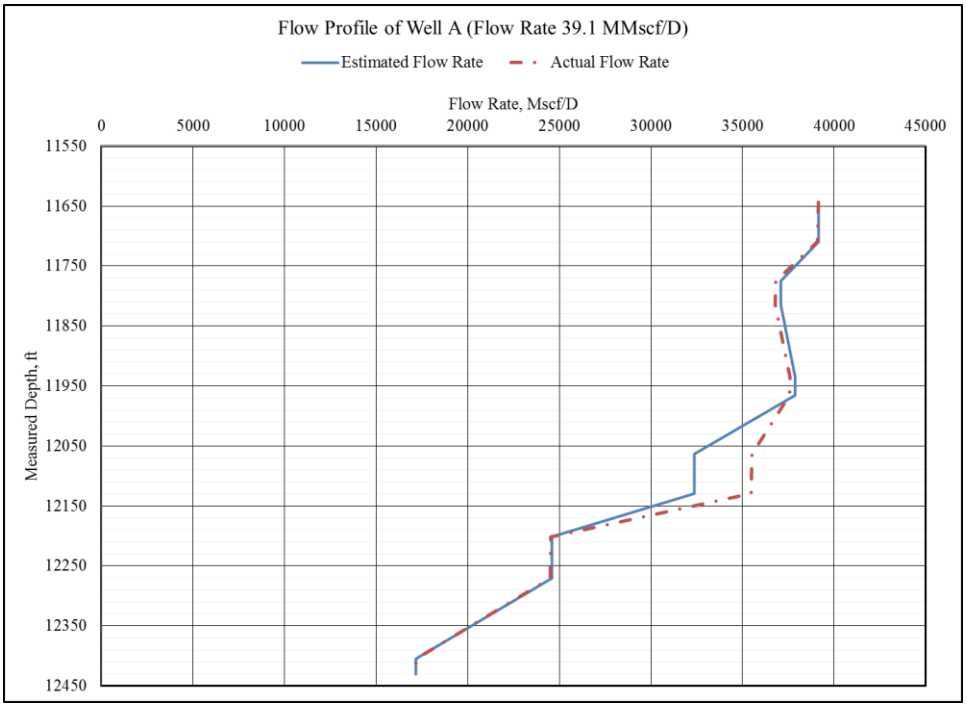

Figure 27: Estimated flow profile of Well A (39.1 MMscf/D case) assuming perforations with outflow are known

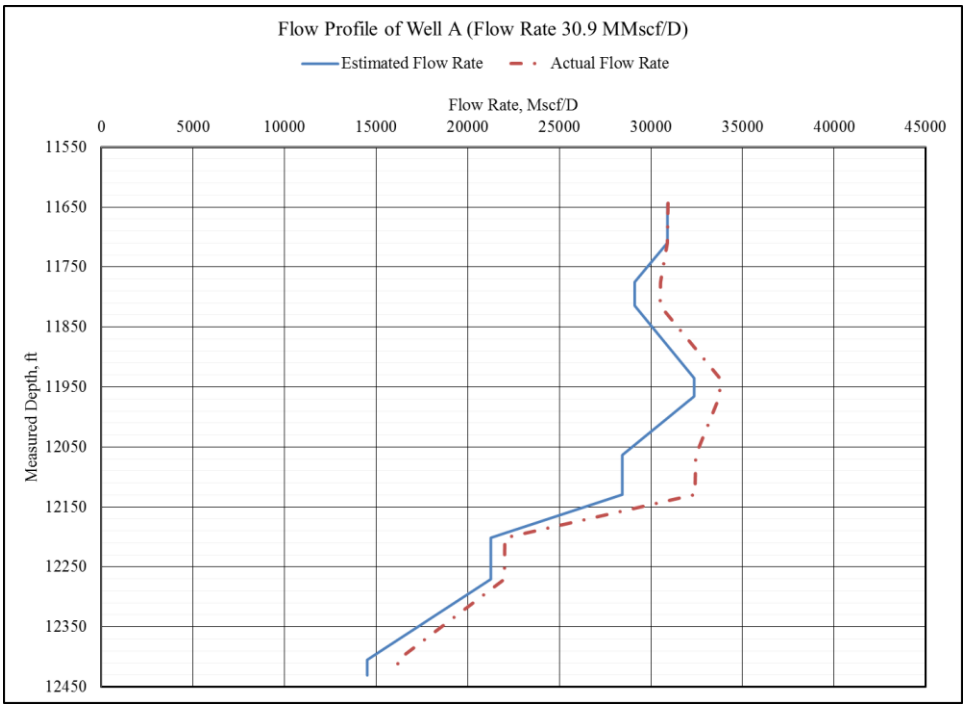

Figure 28: Estimated flow profile of Well A (30.9 MMscf/D case) assuming perforations with outflow are known

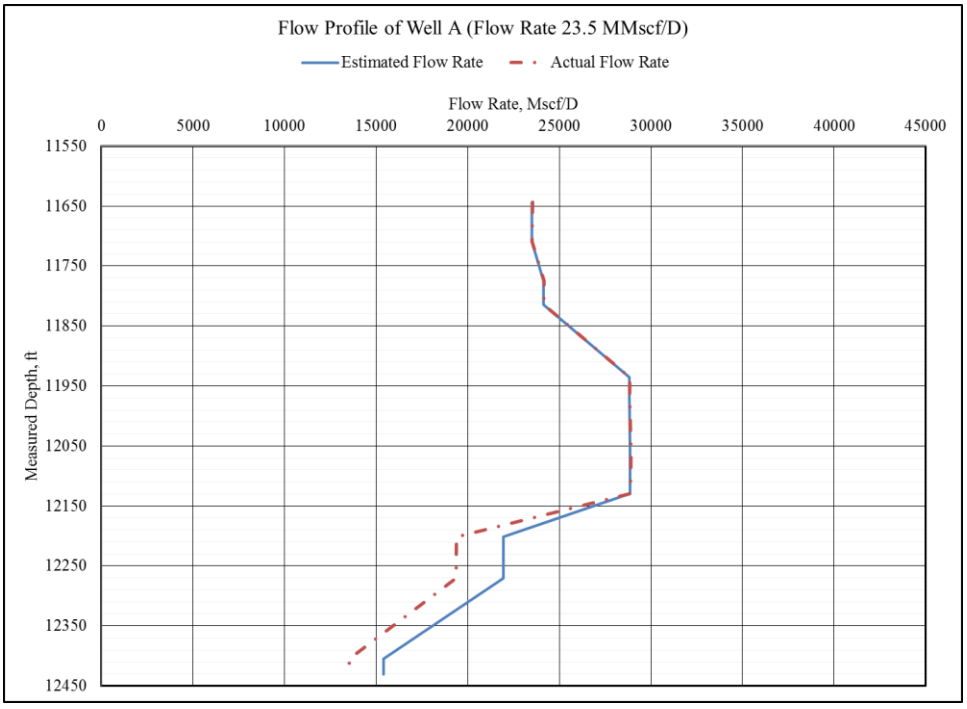

Figure 29: Estimated flow profile of Well A (23.5 MMscf/D case) assuming perforations with outflow are known

4.3. Field Case Study – Well B

Well B is a simpler well compared to Well A. Well B is vertical well with maximum deviation angle being 3.34° and terminal deviation angle is 0.88°. This well is plugged at measured depth of 11,142 ft or true vertical depth of 11,138 ft. The production casing of this well has an internal diameter of 4.778 inch and it runs from surface to total depth of this well. For this well, we used the same geothermal temperature profile as it is in proximity to Well A.

Following table shows the perforation that are currently existing in the wellbore. The average porosity values in table are interpreted by the operator and provided to us. The average permeability and average reservoir pressure of the zones are estimated using the method discussed in subchapter 4.1 using equation (28).

Table 11: Well B Perforations

Perforation	From (ft)	To (ft)	Average Porosity	Estimated Average Permeability (mD)	Estimated Average Reservoir Pressure (psia)
Perforation 3	10,719.04	10,850.24	0.137	3.30	4,422
Perforation 2	10.892.88	10,948.92	0.134	-	-
Perforation 1	10,997.44	11,115.92	0.134	4.51	4,238

For this well, we have access to data from production logging performed in 3 different surface flow rate which are 60.0 MMscf/D, 40.0 MMscf/D and 20.0 MMscf/D. In this study, we consider that only surface flow rate was changed for each case and rest of the external influncers were kept constant.

Following 3 figures show the spinner calibration graph for 3 cases. The highlighted points and the highlighted regression line is for calibration zone 1. Slope and intercept values are presented in the appendix C.

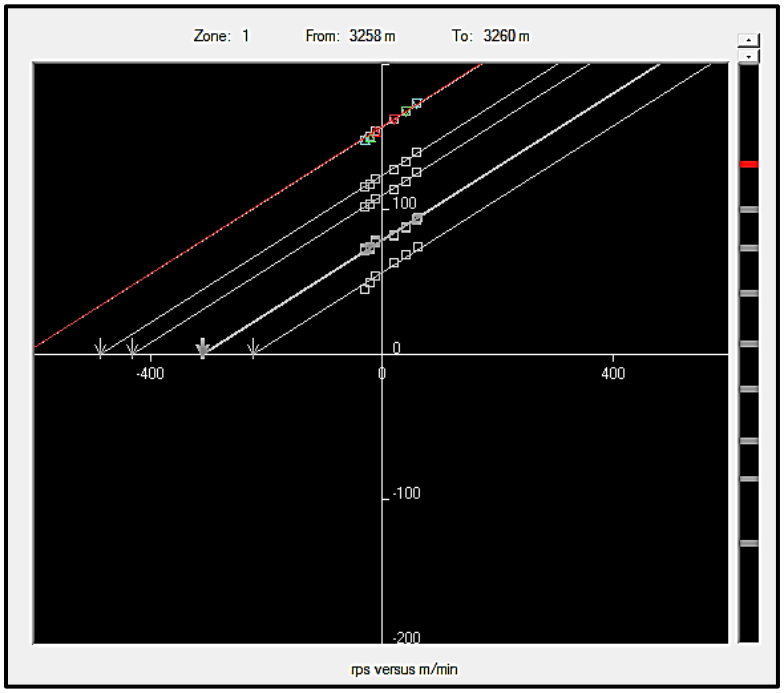

Figure 30: Spinner calibration for Well B 60.0 MMscf/D case

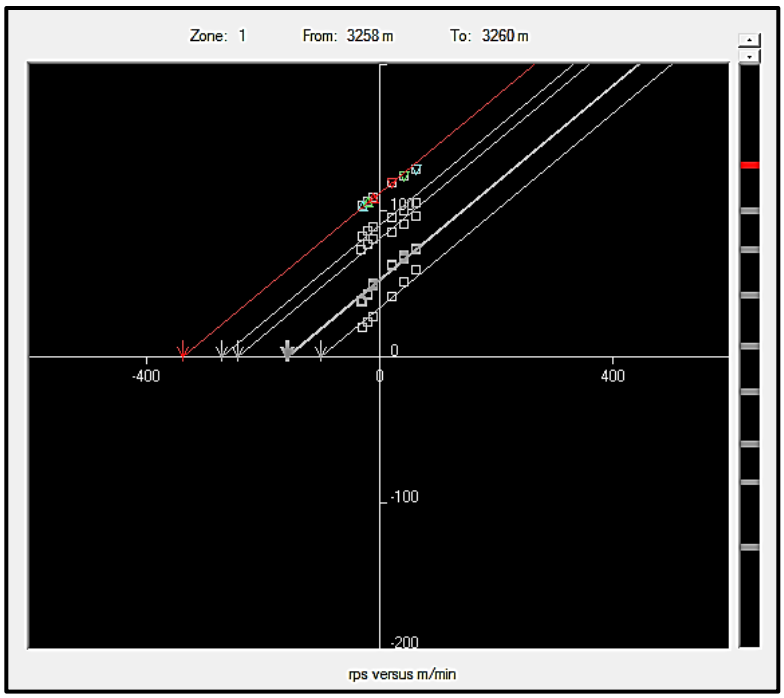

Figure 31: Spinner calibration for Well B 40.0 MMscf/D case

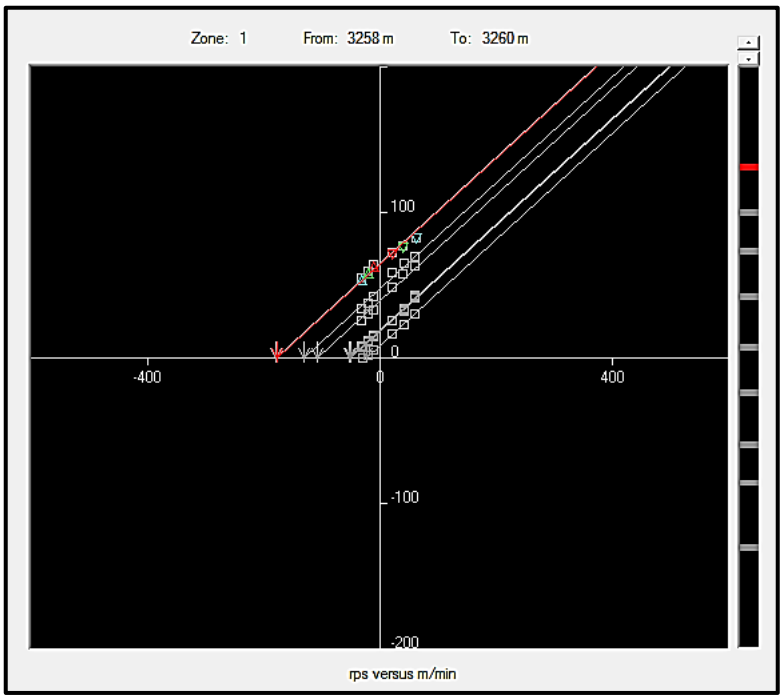

Figure 32: Spinner calibration for Well B 20.0 MMscf/D case

Figure (32) show the temperature profile of the Well B section under investigation while the surface production rate is 60.0 MMscf/D, 40.0 MMscf/D and 20.0 MMscf/D. Geothermal temperature line presented here is the same one used for Well A as both wells are in close proximity.

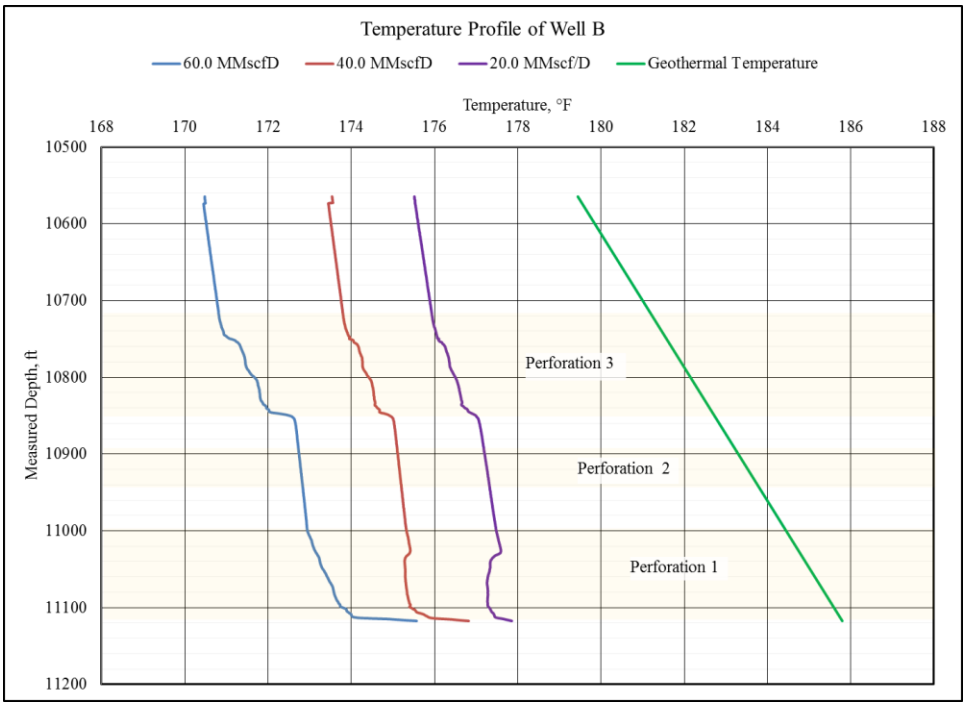

Figure 33: Temperature profile of Well B

Similar to well A, we observed from Figure (32) that wellbore temperature for both cases follow similar shape. But, The temperature for 60.0 MMscf/D case is significantly cooler than the 40.0 MMscf/D case which is subsequently coller compared to 20.0 MMscf/D case. As explained for Well A, this is very typical for a gas well when the reservoir pressure is not too high. In such scenarios, gas cools down as it expands due to Joule-Thompson cooling effect. For larger pressure drop, we see larger temperature drop

when the gas enters the wellbore. As in 60.0 MMscf/D case, the surface flow rate is higher, we can infer that the zonal flow rate is higher than the 40.0 MMscf/D case and 20.0 MMscf/D. Higher flow rate corresponds to larger pressure drop from reservoir to the wellbore for the same reservoir which results cooler fluid entering the wellbore. Thus, the temperature profile for 60.0 MMscf/D case is comparatively colder then 40.0 MMscf/D case and 40.0 MMscf/D case has a colder temperature profile than 20.0 MMscf/D case.

Figure (32) also helps us see that there are significant change in the wellbore fluid temperature in perforation 1 and perforation 3. Which gives us a qualitative idea that both of those perforations have significant production from respective reservoirs. Perforation 2 is a case of outflow from the wellbore to the reservoir (indicated by spinner flowmeter) which means it is a depleted zone and the downhole flowing pressure has to be decreased to lower value in order to produce from that zone. The model developed in this study is based on mixing cup approach which requires inflow from the reservoir into the wellbore, thus making the model invalid for perforation 2. Another observation that can be inferred from the figure (32) is that change of fluid temperature perforation 2 due to incoming fluid of different temperature is negligible. This situation qualitatively tells us that the flow rate from this zone is very small compared to other higher producing zone. Also, in the interpreted spinner log agrees with this conclusion by showing that the absolute value of flow rate in perforation 2 is is negligible. So, for this analysis, perforation 2 is neglected.

Following figure shows the pressure profile of the wellbore section under investigation,

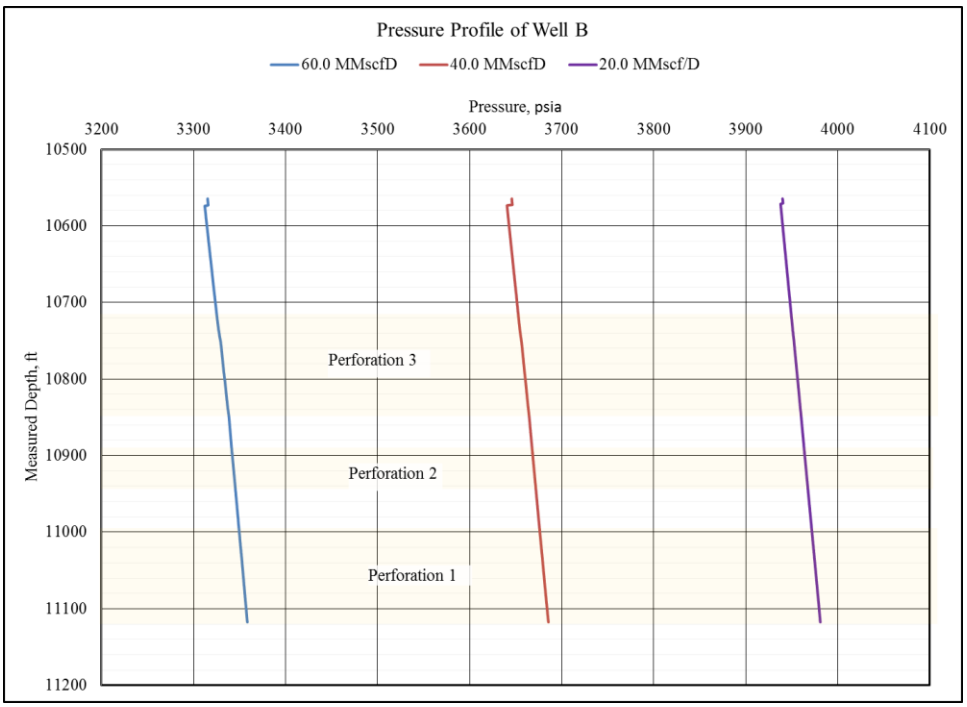

Figure 34: Pressure profile of Well B

Utilizing the the temperature profile and pressure profile shown above, we get the zonal flow allocation presented in figure (34), figure (35) and figure (36).

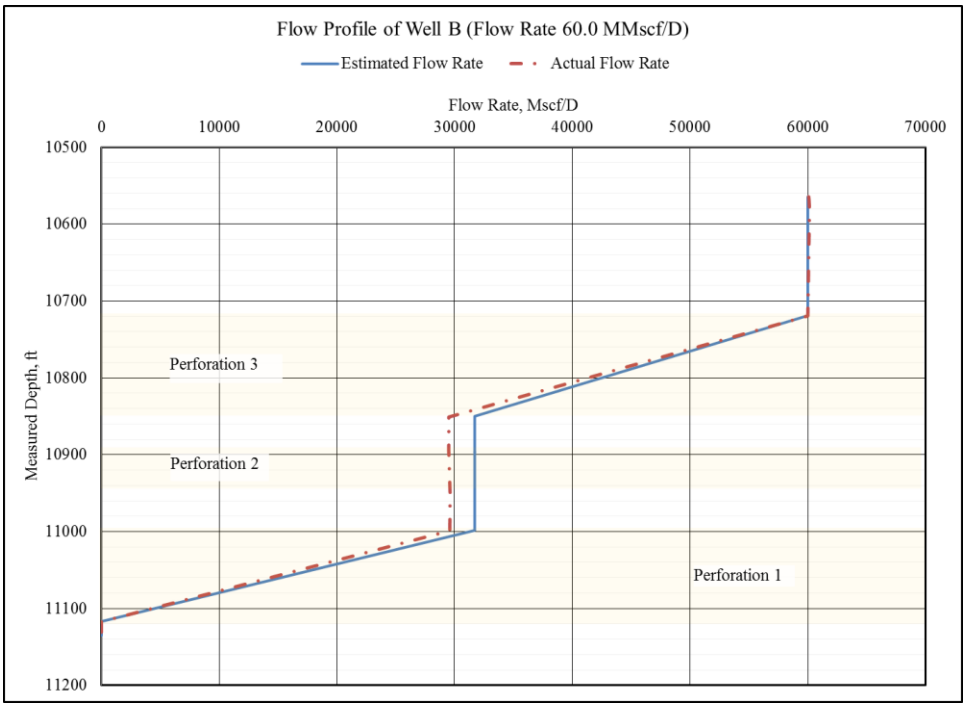

Figure 35: Estimated flow profile of Well B (60.0 MMscf/D case)

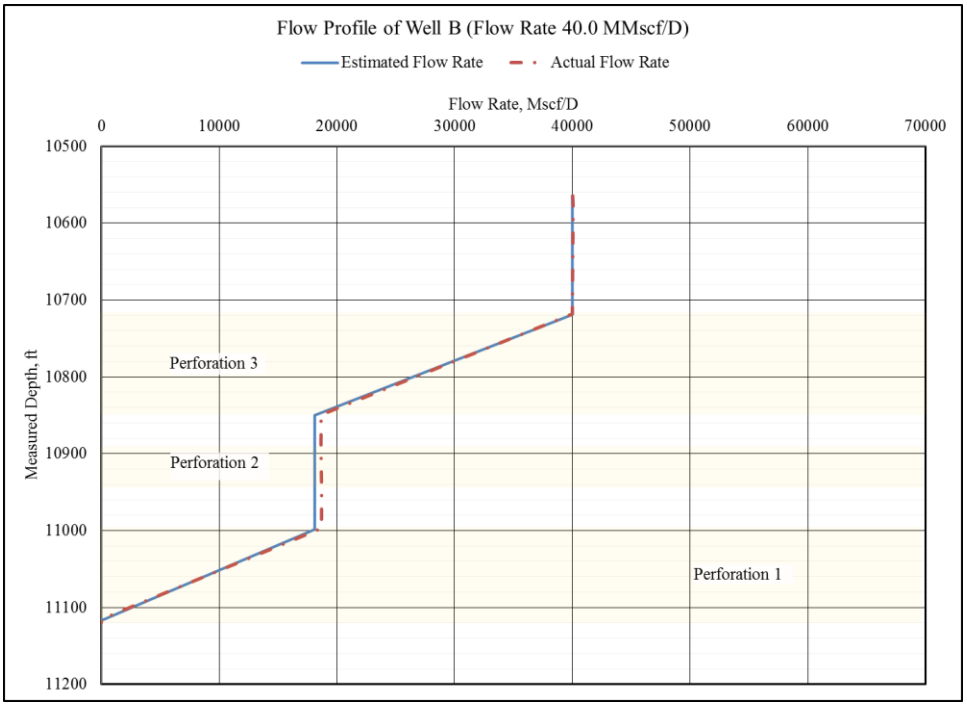

Figure 36: Estimated flow profile of Well B (40.0 MMscf/D case)

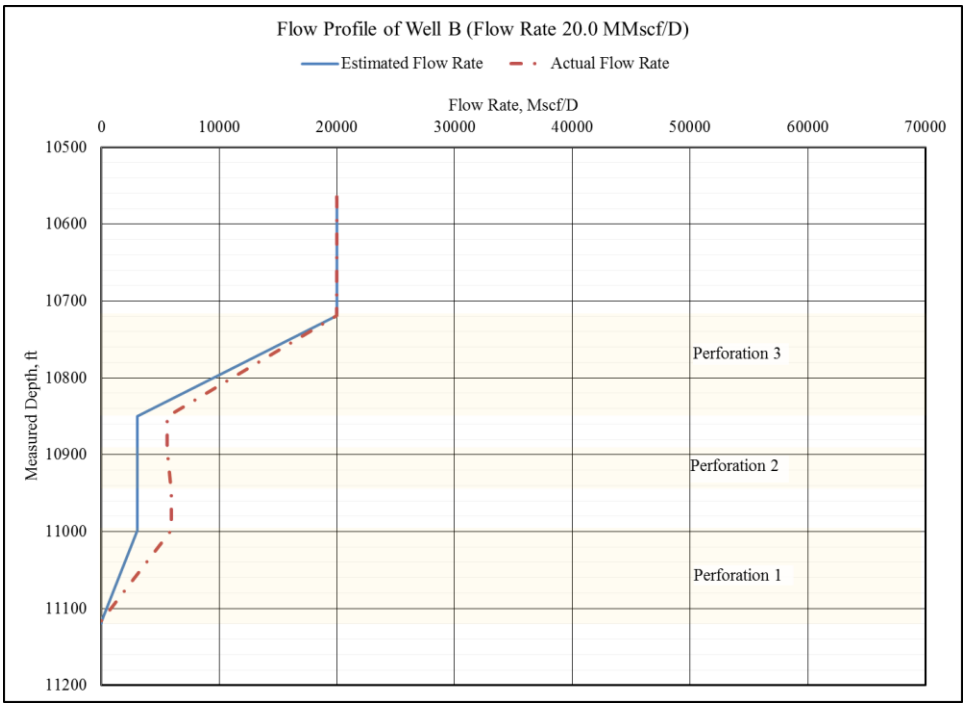

Figure 37: Estimated flow profile of Well B (20.0 MMscf/D case)

4.4. Field Case Study – Well C

Well C is S-Type well with maximum deviation angle being 34.11° and terminal deviation angle is 5.16°. Total measured depth of 12,661 ft or true vertical depth of 12,046 ft. The production casing of this well has an internal diameter of 4.778 inch and it runs from surface to total depth of this well.

For this well, we have an unique scenario as we have access to the temperature and pressure data of the rathole which is about 200ft deeper than the deepest perforation interval. A logical assumption can be made that the temperature of the rathole is very close to the geothermal temperature at that depth if not the same. With that assumption, we shifted the geothermal temperature line by +4°F to match that rathole temperature but kept

the same geothermal gradient used in previous two wells. Such an assumption leads to a good match of geothermal temperature and the rathole temperature as seen in figure (41).

Following table shows the perforation that are currently existing in the wellbore. The average porosity values in table are interpreted by the operator and provided to us. The average permeability and average reservoir pressure of the zones are estimated using the method discussed in previous subchapter.

Table 12: Well C Perforations

Perforation	From (ft)	To (ft)	Average Porosity	Estimated Average Permeability (mD)	Estimated Average Reservoir Pressure (psia)
Perforation 6	11040.48	11083.12	0.158	140.00	3,792
Perforation 5	11119.2	11243.84	0.158	10.50	3,802
Perforation 4	11256.96	11404.56	0.147	0.44	3,751
Perforation 3	11420.96	11466.88	0.147	-	-
Perforation 2	11489.84	11611.2	0.122	-	-
Perforation 1	11637.44	11703.04	0.122	5.20	3776.4

For this well, we have access to data from production logging performed in 3 different surface flow rate which are 64.0 MMscf/D, 40.0 MMscf/D and 28.5 MMscfD. In this study, we consider that only surface flow rate was changed and rest of the external influncers are constant.

Following 3 figures show the spinner calibration graph for 3 cases. The highlighted points and the highlighted regression line is for calibration zone 1. Slope and intercept values are presented in the appendix C.

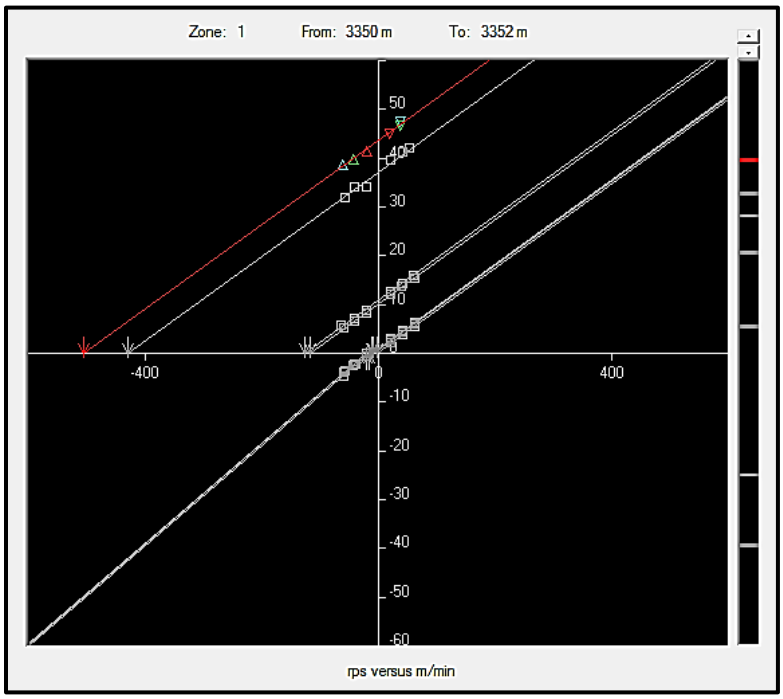

Figure 38: Spinner calibration for Well C 64.0 MMscf/D case

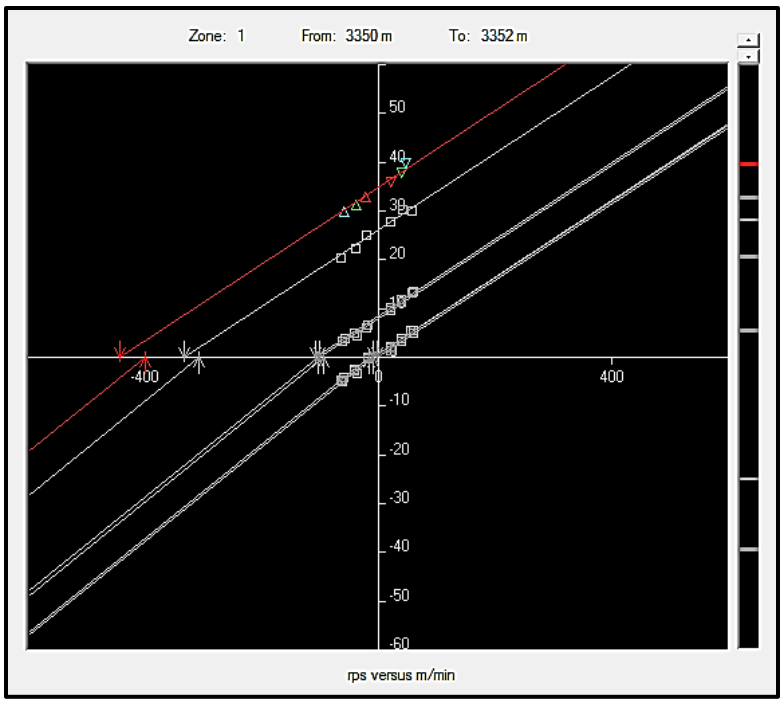

Figure 39: Spinner calibration for Well C 40.0 MMscf/D case

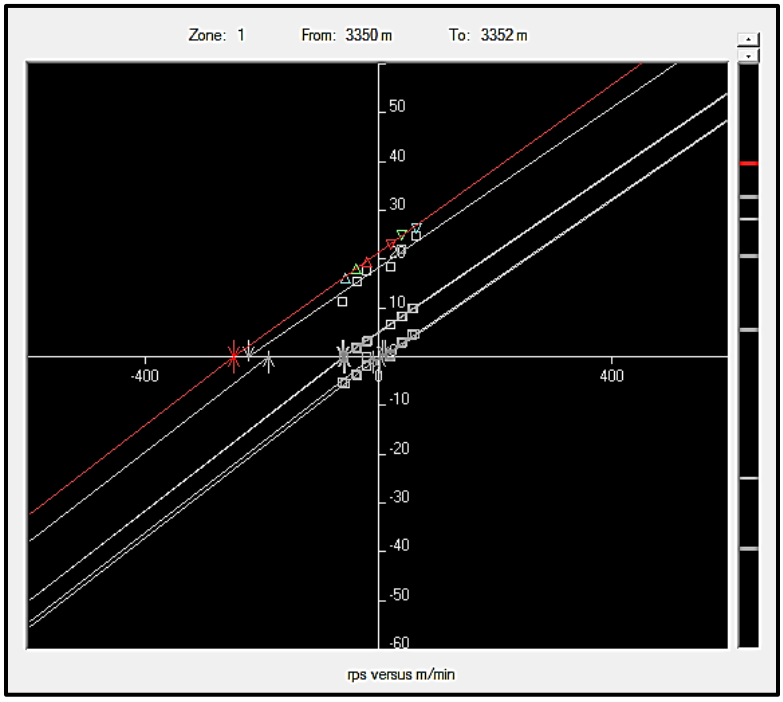

Figure 40: Spinner calibration for Well C 28.5 MMscf/D case

Following graph show the temperature profile of the Well B section under investigation while the surface production rate is 40 MMscf/D and 40.0 MMscf/D. Geothermal temperature line presented here is the has the same gradient as other two wells but shifted +3°F to match rathole temperature.

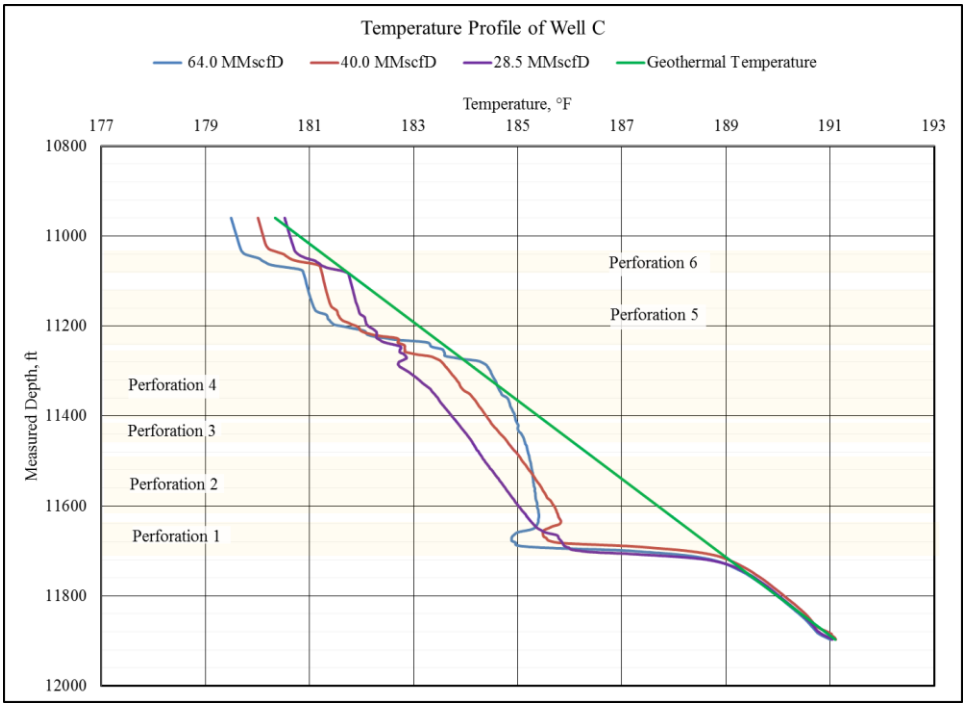

Figure 41: Temperature profile of Well C

Well C is more complex compared to well A and well B. It has 6 closely placed perforations. We observe from Figure (41) that wellbore temperature follow a slightly different shape but general trend is similar for all the flow rates. Across perforation 1, perforation 5 and perforation 6, the wellbore fluid temperature for 40.0 MMscf/D case is significantly cooler than the 28.5 MMscf/D case while 64.0 MMscf/D case is cooler compared to 40.0 MMscf/D case. As explained in the discussions for Well A and Well B,

we know that this phenomena means that we have higher flow rate from those zones in 64.0 MMscf/D case than 40.0 MMscf/D case and 28.5 MMscf/D. So, We can get to a qualitative conclusion that perforation 1, perforation 5 and perforation 6 has the maximum contribution the the surface flow rate from this well.

For perforation 2 and perforation 3, there are no sharp temperature change across the perforation. So, another qualitative conclusion can be made that those zones produce significantly lower compared to other high producing zones. The interpreted spinner log agrees with this conclusion by showing that the absolute value of flow rate in perforation 2 and perforation 3 is negligible. So, for this analysis, these 2 perforations are neglected.In perforation 4, we see a sharp change near the top of the perforation indicating that most of the production from this zone is basically coming from top 20 feet of the perforation. So, this zone is not neglected in our analysis.

Figure (42) shows the pressure profile of the wellbore section under investigation. Figure (42) shows us that there are significant changes in the wellbore flowing pressure below the deepest perforation (perforation 1). The reason of this sharp change in slope in each of the cases is the change in fluid. Below perforation 1, we have the rathole, which is usually filled with liquid eg, water or condensate. Thus, in rathole we have larger pressure drop per unit depth while the pressure drop becomes less steep as soon as we come up to the bottom of perforation where reservoir gas starts coming into the wellbore and flow upwards.

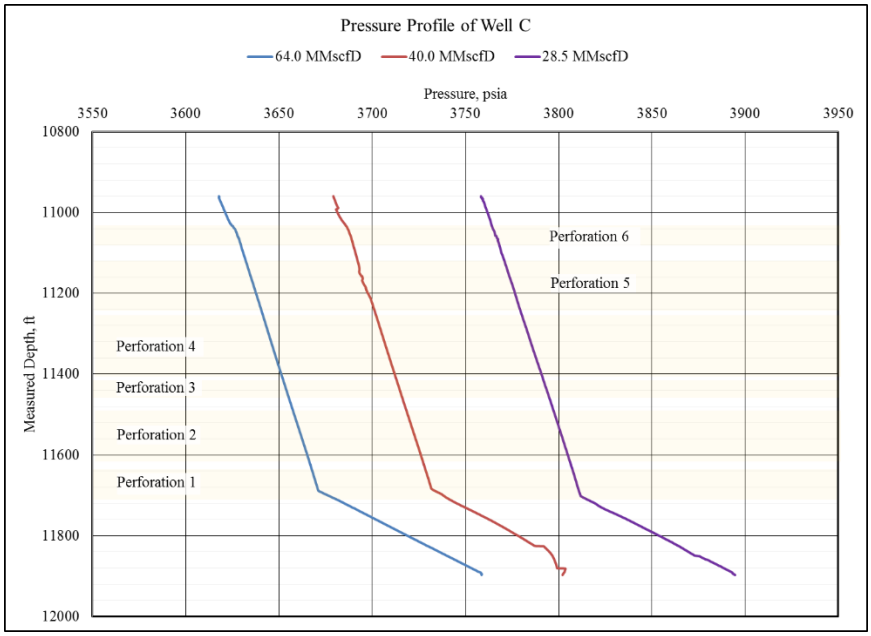

Figure 42: Pressure profile of Well C

Utilizing the the temperature profile and pressure profile shown above, we get the zonal flow allocation presented in figure (43), figure (44) and figure (45).

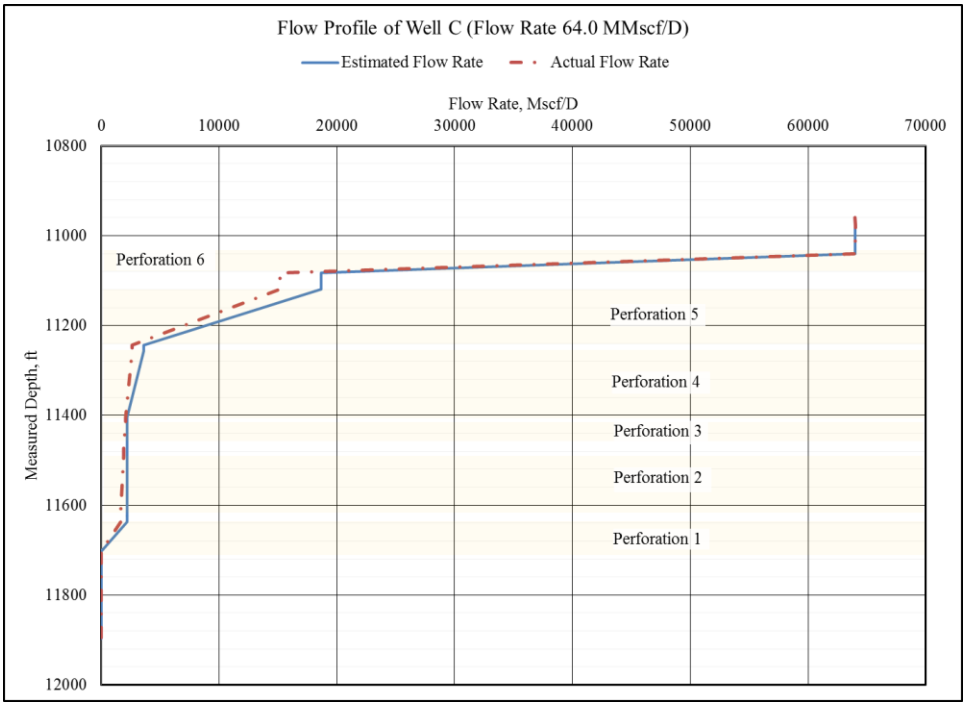

Figure 43: Estimated flow profile of Well C (64.0 MMscf/D case)

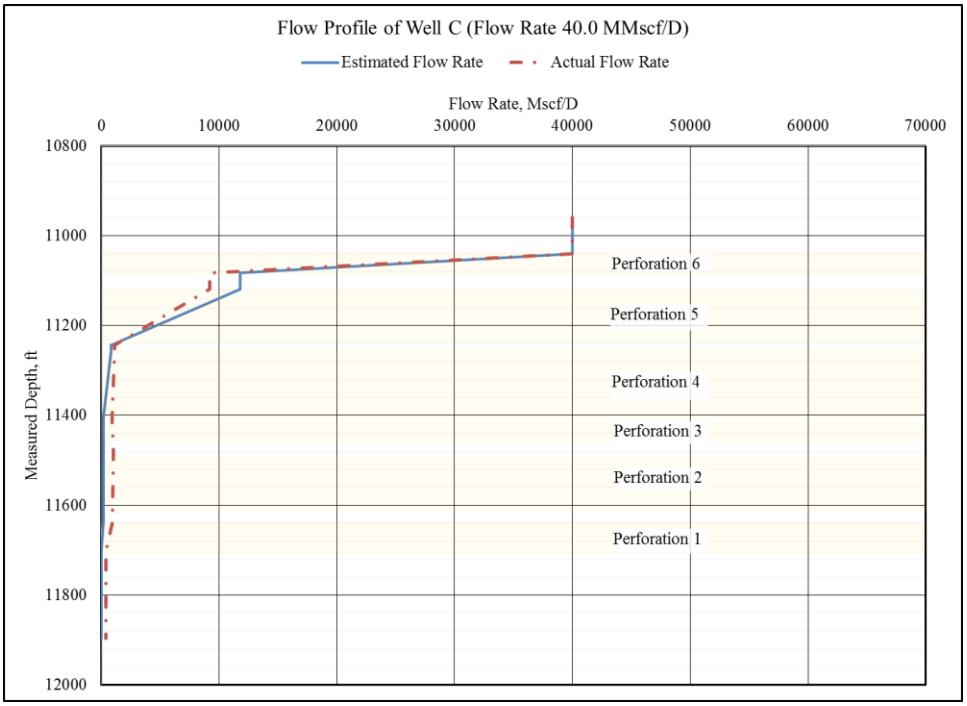

Figure 44: Estimated flow profile of Well C (40.0 MMscf/D case)

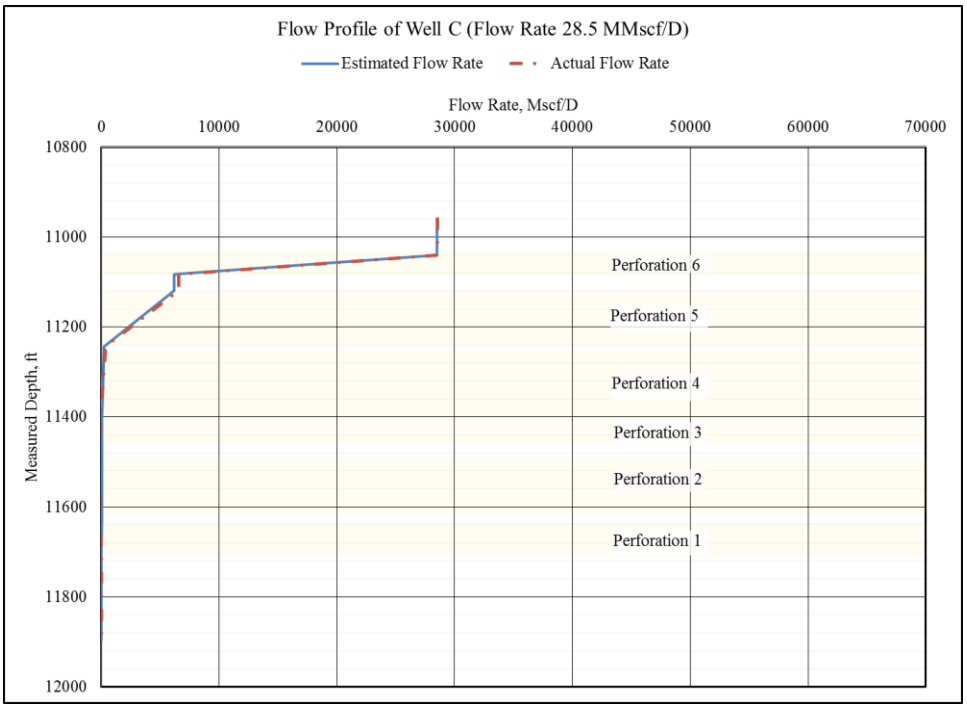

Figure 45: Estimated flow profile of Well C (28.5 MMscf/D case)

4.5. Field Case Study – Well A (Using Estimated Pressure Profile)

As discussed in subchapter 3.4, wellbore pressure data does not affect the model output significantly as long as the error is is not significant. This conclusion promts us to attempt a study to verify if using estimated pressure profile of a gas well results in reasonable estimation of flow profile given that we have measurements of temperature throughout wellbore.

We calculated fluid pressure throughout the wellbore of Well A using the method discussed in subchapter 3.2 starting from the shallowest measurement available. Figure (47) shows the result of that test. We can see that the flow profile is reasonably similar to the estimate done from measure pressure profile in figure (24).

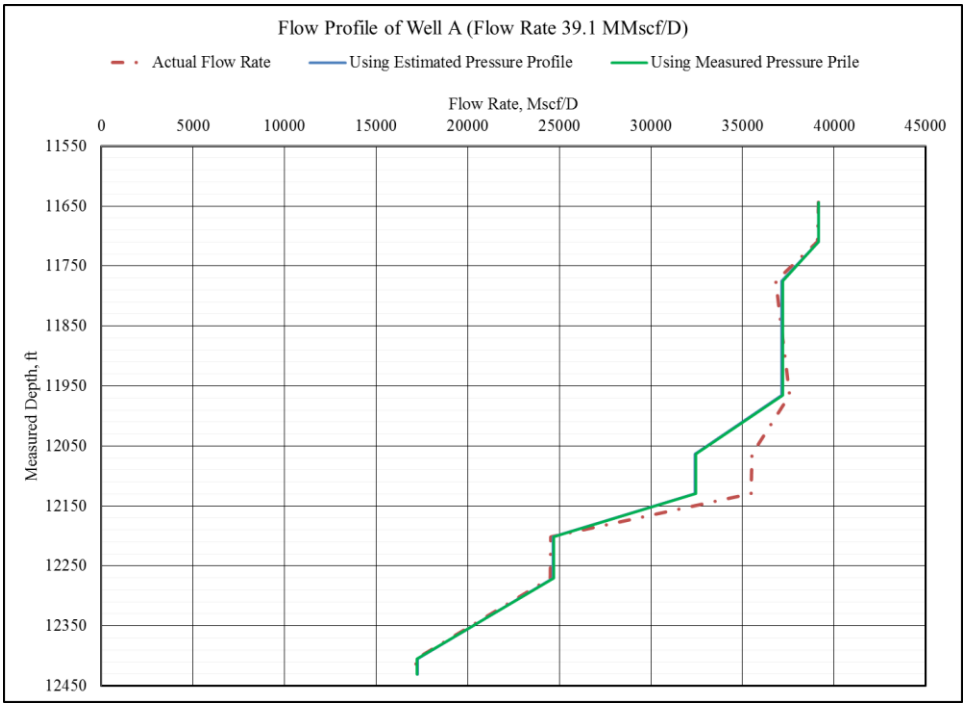

Figure 46: Estimated flow profile of Well A (39.1 MMscf/D case) using estimated pressure profile

4.6. Limitation of the Model

Small changes in wellbore fluid temperature or sand-face temperature ends up being a big change in percentage error of zonal flow rate for zones with smaller flow rate and very small fluid temperature change across the zone. Zones with larger flow rates are less susceptible to such effects.

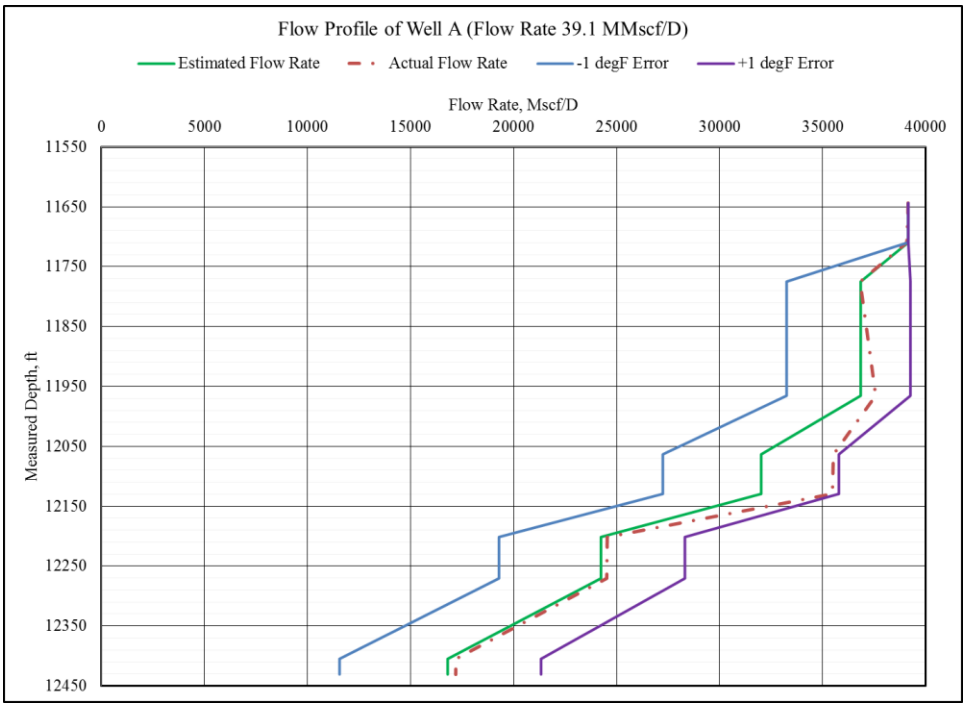

Figure 47: Estimated flow profile of Well A (39.1 MMscf/D case) illustrating the sensititivity to error in wellbore fluid temperature

Table 13: Error in zonal flow rate of Well A if error introduced in wellbore fluid temperature

Changes in Well A Zonal Flow Rate for Error in Fluid Temperature				
Perforation	Actual Flow Rate (Mscf/D)	Model Estimated Flow Rate (Mscf/D)	-1 degF Error	+1 degF Error
7	2304	2308	156.00%	-104.58%
5	2102	4828	24.40%	-28.06%
4	10961	7772	2.23%	-3.92%
3	7333	7438	4.02%	-6.13%

5. CONCLUSIONS AND RECOMMENDATIONS

5.1 Conclusions

This study primarily focused on developing and testing an analytical approach that can estimate zonal flow rate contributions from different zones in a multi-zone completion where temperature and pressure profile is known. We developed the model based on basic energy balance in a control volume within the wellbore and made it suitable for using in producing sections of a well. The approach we took to develop this model is known as the mixing-cup approach, which is based on the idea that inflow fluid from the reservoir mixes with the fluid already inside the wellbore and reaches a thermal equilibrium. To test the model we developed, we generated a synthetic dataset for a typical conventional gas well which was assumed to be producing from multiple zones. This synthetic dataset was generated from industry standard methods that were discussed in body of this study. Afterwards, we used the generated dataset and estimated the flow profile of the the well that we assumed. We performed sensitivity tests to check the influence of different parameters on the output of the model.

The biggest challenge for our model is measuring or estimating sand-face temperature. Measuring actual sand-face temperature in the fluid entry points can be a very difficult ask which requires advanced technical solutions and significant monetary investments in planning the completion. So, such measurement devices are really uncommon in practical field use in current industry state. For cases where sand-face

temperature is unknown, published methods of estimating sand-face temperature can be used. In this study, we used the model developed by Xu et al. (2018). This method requires flow rate of the zone as an input. But, the objective of developing our analytical model is to estimate the unknown zonal flow rate. This situation leads us to developing an iterative procedure of solving our model. The iterative method is discussed in details in the body of this study and this methos works really well in minimizing errors to get a good match with actual flow profile of the well if rest of the parameters are known.

Results of the sensitivity tests show that wellbore fluid temperature and sand-face fluid temperature can be very influencial to our model output. Small errors in either temperature measurement or estimates can lead to significant errors in the estimation of zonal flow rates. Specific heat capacity of the fluid can also impact the output significantly if it is not measured or assumed correctly. We noticed that wellbore pressure does not impact the model output significantly. If we are within the accuracy range of any common pressure gauges, we can get pretty good estimates of the zonal flow rates.

We have validated our model against field data from 3 conventional gas wells. We used temperature and pressure profile of those wells and estimated a flow profile using the model we developed in this study. These validation checks were done for 3 different surface flow rates of each well. The estimated flow profiles from the model were checked against spinner flowmeter data from those wells for each different surface flow rates. These spinner flowmeter data was interpreted by us using a commercial production logging software. The results of these field case studies show that our model works pretty

well if the assumptions are within a certain range. For zones with larger production rates, the model works more accurately. But, if a zone is producing a small portion of the total well production or the fluid temperature change across that zone is minimal, it becomes very difficult to estimate the flow rate from that zone. We showed such an example in field case study of Well A and discussed this limitation with a sensitivity study comparing the errors in the estimates of flow rates in different zones of that well based on the input error in temperature measurements or estimates for that well.

We also checked the opportunity of using pressure profile estimated from surface pressure and flow rates using simple industry standard approach as the sensitivity of pressure profile is lower compared to temperature profile. Such a test allows the use of our model to be easier and more realistic as pressure gauges or distributed pressure sensors are less common in the field than distributed temperature sensors. Our test shows that such an estimate of pressure profile can eventually lead to very good estimates of zonal flow allocation if temperature measuremts are accurate.

In conclusion, the model we developed can provide operators around the world with a robust yet very simple solution to the challenge of estimating zonal flow contribution. Use of distributed temperature sensors are increasing day by day, and such sensors can be source of real time temperature profile with hig accuracy that can be used conveniently as the input for the model developed in this study to get reasonable allocation flow rate to different zones. Although, The model discussed in this study was developed

having a gas well in mind, I can also be applicable for single phase oil and even two-phase flow if all the parameters are known.

5.2 Recommendations for Future Work

This study involved developing the zonal flow allocation model for very simple case with some simplifying assumptions. These a lot of room for improvement if future work is done on this model. Following list shows some of the recommendations that can improve this model and develop a more robust and versatile method for widespread industry usage:

1. Investigating feasibility of such approach in two phase production cases.
2. Using the actual value of specific heat capacity at different temperature and pressure rather than using a constant value.
3. Accounting for heat transfer between formation and wellbore fluid within the producing section of the well.
4. Exploring the possibility of expanding this model to use in horizontal wells.
5. Improve the model for use in zones where temperature anomaly is minimal.

REFERENCES

Barrett, E. E., Abbasy, I., Wu, C. R., You, Z., & You, P. B. (2012, January 1). Treatment of Temperature and Pressure Profiles along the Wellbore to Determine Gas Rate. Presented at SPE International Production and Operations Conference & Exhibition, 14-16 May, Doha, Qatar. SPE-152039-MS. 1-12. http://dx.doi.org/doi:10.2118/152039-MS.

Bird, J. M. (1954, January 1). Interpretation of Temperature Logs in Water- and Gas-injection Wells and Gas-producing wells. Presented at American Petroleum Institute Drilling and Production Practice, 1 January, New York, New York. API-54-187. 1-9.

Bird, J. M., & Frost, N. (1965, January 1). Formation Productivity Evaluation From Temperature Logs. Presented at Society of Petrophysicists and Well-Log Analysts 6th Annual Logging Symposium (Volume II), 4-7 May, Dallas, Texas. 1-18.

Bird, J.M. and Frost, N. 1966. Formation Productivity Evaluation From Temperature Logs. Society of Petroleum Engineers Journal of Petroleum Technology 18 (3): 301—305. SPE-1350-PA. http://dx.doi.org/10.2118/1350-PA.

Brown, G. A. (2006, January 1). Monitoring Multilayered Reservoir Pressures and GOR Changes Over Time Using Permanently Installed Distributed Temperature Measurements. Presented at SPE Annual Technical Conference and Exhibition, 24-27 September, San Antonio, Texas, USA. SPE-101886-MS. 1-14. http://dx.doi.org/doi:10.2118/101886-MS.

Brown, G. A., & Hartog, A. (2002, November 1). Optical Fiber Sensors in Upstream Oil & Gas. Society of Petroleum Engineers Journal of Petroleum Technology 54 (11): 63—65. SPE-79080-JPT. https://doi.org/10.2118/79080-JPT.

Curtis, M. R., & Witterholt, E. J. (1973, January 1). Use Of The Temperature Log For Determining Flow Rates In Producing Wells. Presented at Fall Meeting of the Society of Petroleum Engineers of AIME, 30 September-3 October, Las Vegas, Nevada. SPE-4637-MS. 1-12. https://doi.org/10.2118/4637-MS.

Dranchuk, P. M., Purvis, R. A., & Robinson, D. B. (1973, January 1). Computer Calculation Of Natural Gas Compressibility Factors Using The Standing And Katz Correlation. Presented at Petroleum Society of Canada Annual Technical Meeting, May 8 - 12, Edmonton. PETSOC-73-112. 1-17. https://doi.org/10.2118/73-112.

Grattan, K.T.V., Meggitt, B.T. 1995. *Optical Fibre Sensor Technology*, London, Chapman & Hall.

Hasan, A.R., Kabir, C.S. 2002. *Fluid Flow and Heat Transfer in Wellbores*. Richardson, TX: SPE Textbook Series.

Hasan, A. R., Kabir, C.S. , X. Wang. 2009. A Robust Steady-State Model for Flowing-Fluid Temperature in Complex Wells. SPE Production & Operations 24 (02) (May 2009): 269-276. SPE-109765-PA. https://doi.org/10.2118/109765-PA.

Hasan, A.R., Sohel, R.N., Wang, X. 2017.Estimating Zonal Flow Contributions in Deep Water Assets From Pressure and Temperature Data. *Proc.*, ASME International Conference on Offshore Mechanics and Arctic Engineering, Volume 8: Polar and Arctic Sciences and Technology; Petroleum Technology ():V008T11A055. 1-12. https://doi.ogr/:10.1115/OMAE2017-62537.

Hill, A.D. 1990. *Prouction Logging-Theoretical and Interpretive Elements*, Vol. 14, 28-29. Richardson, TX: SPE Monograph Series, Society of Petroleum Engineers.

Johnson, D. O., Sierra, J. R., Kaura, J. D., & Gualtieri, D. (2006, January 1). Successful Flow Profiling of Gas Wells Using Distributed Temperature Sensing Data. Presented at Society of Petroleum Engineers Annual Technical Conference and Exhibition, 24-27 September, San Antonio, Texas, USA. SPE-103097-MS. 1-16. https://doi.org/10.2118/103097-MS.

Kabir, C. S., Izgec, B., Hasan, A. R., Wang, X., & Lee, J. (2008, January 1). Real-Time Estimation of Total Flow Rate and Flow Profiling in DTS-Instrumented Wells. Presented at International Petroleum Technology Conference, 3-5 December, Kuala Lumpur, Malaysia. IPTC-12343-MS. 1-10. https://doi.org/10.2523/IPTC-12343-MS.

Kading, H. W., & Hutchins, J. S. (1969, January 1). Temperature Survey: The Art of Interpretation. Presented at American Petroleum Institute Drilling and Production Practice, 1 January, Washington D.C. API-69-001. 1-20.

Karaman, O. S., Kutlik, R. L., & Kluth, E. L. (1996, January 1). A Field Trial to Test Fiber Optic Sensors for Downhole Temperature and Pressure Measurements, West Coalinga Field, California. Presented at Society of Petroleum Engineers Western Regional Meeting, 22-24 May, Anchorage, Alaska. SPE-35685-MS. 1-7. https://doi.org/10.2118/35685-MS.

Kunz, K. S., & Tixier, M. P. (1955, January 1). Temperature Surveys in Gas Producing Wells. Presented at AIME Annual Meeting 13-17 Feb, Chicago. SPE-472-G. 1-9.

Lee, A. L., Gonzalez, M. H., & Eakin, B. E. (1966, August 1). The Viscosity of Natural Gases. Journal of Petroleum Technology 18 (08): 997-1000. SPE-1340-PA. https://doi.org/10.2118/1340-PA.

Lequime, M., Lecot, C., Jouve, P., Pouleau, J., (1991, August 1). Fiber optic pressure and temperature sensor for down-hole applications, *Proc.*, SPIE 1511, Fiber Optic Sensors: Engineering and Applications. https://doi.org/10.1117/12.45997.

Muradov, K. M., & Davies, D. R. (2011, January 1). Application of Distributed Temperature Measurements to Estimate Zonal Flow Rate and Pressure. Presented at International Petroleum Technology Conference, 15-17 November, Bangkok, Thailand. IPTC-15215-MS. 1-17. https://doi.org/10.2523/IPTC-15215-MS.

Nowak, T. J. (1953, August 1). The Estimation of Water Injection Profiles From Temperature Surveys. Journal of Petroleum Technology 5 (08): 203-212. SPE-953203-G. https://doi.org/10.2118/953203-G.

Ouyang, L.-B., & Belanger, D. L. (2006, May 1). Flow Profiling by Distributed Temperature Sensor (DTS) System - Expectation and Reality. Society of Petroleum Engineers Production & Operations 21 (02): 269-281. SPE-90541-PA. https://doi.org/10.2118/90541-PA.

Peacock, D. R. (1965, January 1). Temperature Logging. Presented at Society of Petrophysicists and Well-Log Analysts 6th Annual Logging Symposium (Volume I), 4-7 May, Dallas, Texas. SPWLA-1965-F. 1-18.

Ramey, H. J. (1962, April 1). Wellbore Heat Transmission. Society of Petroleum Engineers Journal of Petroleum Technology 14 (04): 427-435. SPE-96-PA. https://doi.org/10.2118/96-PA.

Romero-Juarez, A. (1969, December 1). A Note on the Theory of Temperature Logging. Society of Petroleum Engineers Journal 9 (04): 375-377. SPE-2464-PA. https://doi.org/10.2118/2464-PA.

Schonblom, J. E. (1961, January 1). Quantitative Evaluation Of Temperature Logs In Flowing Gas Wells. Society of Petroleum Engineers. SPE-238-MS. 1-36.

Steffensen, R. J., & Smith, R. C. (1973, January 1). The Importance of Joule-Thomson Heating (or Cooling) in Temperature Log Interpretation. Presented at Society of Petroleum Engineers Fall Meeting of the Society of Petroleum Engineers of AIME, 30 September-3 October, Las Vegas, Nevada. SPE-4636-MS. 1-15. https://doi.org/10.2118/4636-MS.

Venkatraman, A., Hasan, A. R., Sohel, R. H., Patni, S., Elshahawi, H., Yousif, M. H., & Abbasi, F. R. (2015, September 28). Quantifying Flow Rates From Temperature and Pressure Measurements in Deepwater Wells. Presented at Society of Petroleum Engineers Annual Technical Conference and Exhibition, 28-30 September, Houston, Texas, USA. SPE-174977-MS. 1-12. https://doi.org/10.2118/174977-MS.

Wang, X., Bussear, T. R., & Hasan, A. R. (2010, January 1). Technique To Improve Flow Profiling Using Distributed-Temperature Sensors. Presented at Society of Petroleum Engineers Latin American and Caribbean Petroleum Engineering Conference, 1-3 December, Lima, Peru. SPE-138883-MS. 1-10. https://doi.org/10.2118/138883-MS.

Xu, B., Kabir, S., & Hasan, A. R. (2018, April 22). Modeling Coupled Nonisothermal Reservoir/Wellbore Flow Behavior in Gas Reservoir Systems. Presented at Society of Petroleum Engineers Western Regional Meeting, 22-26 April, Garden Grove, California, USA. SPE-190067-MS. 1-19. https://doi.org/10.2118/190067-MS.

Yoshioka, K., Zhu, D., & Hill, A. D. (2007, January 1). A New Inversion Method to Interpret Flow Profiles From Distributed Temperature and Pressure Measurements in Horizontal Wells. Presented at Society of Petroleum Engineers Annual Technical Conference and Exhibition, 11-14 November, Anaheim, California, U.S.A. SPE-109749-MS. 1-23. https://doi.org/10.2118/109749-MS.

Yoshioka, K., Zhu, D., Hill, A. D., Dawkrajai, P., & Lake, L. W. (2005, January 1). A Comprehensive Model of Temperature Behavior in a Horizontal Well. Presented at Society of Petroleum Engineers Annual Technical Conference and Exhibition, 9-12 October, Dallas, Texas. SPE-95656-MS. 1-15. https://doi.org/10.2118/95656-MS.

Yoshioka, K., Zhu, D., Hill, A. D., & Lake, L. W. (2009, November 1). A New Inversion Method to Interpret Flow Profiles From Distributed Temperature and Pressure Measurements in Horizontal Wells. SPE Production & Operations 24 (04): 510-521. SPE-109749-PA. https://doi.org/10.2118/109749-PA.

APPENDIX A

Fluid Properties Calculation

To begin, TVD is calculated from the assumed measured depth,

$$TVD = MD * sin\alpha \dots\dots\dots (A1)$$

Critical pressure and critical temperature of the assumed gas is calculated using Standing's (1977) expression,

$$p_{pc} = 677 + 15.0\gamma_{gHC} - 35.7\gamma_{gHC}^2 \dots\dots\dots (A2)$$

$$T_{pc} = 168 + 325\gamma_{gHC} - 12.5\gamma_{gHC}^2 \dots\dots\dots (A3)$$

From critical pressure and critical temperature of the assumed gas, pseudoreduced pressure and pseudoreduced temperature is calculated using following expressions,

$$p_{pr} = \frac{p}{p_{pr}} \dots\dots\dots (A4)$$

$$T_{pr} = \frac{T}{T_{pr}} \dots\dots\dots (A5)$$

Density of the fluid can be calculated by following expression,

$$\rho_{pr} = 0.27\left[\frac{p_{pr}}{ZT_{pr}}\right] \dots\dots\dots (A6)$$

Using DPR method by Dranchuk et al (1973) to calculate Z-factor,

$$f(\rho_{pr}) = a\rho_{pr}^6 + b\rho_{pr}^3 + c\rho_{pr}^2 + d\rho_{pr} + e\rho_{pr}^3(1 + f\rho_{pr}^2)e^{-f\rho_{pr}^2} - g \dots\dots\dots (A7)$$

$$a = a_{ro} \dots\dots\dots (A8)$$

$$b = b_{ro1}T_{pr} - b_{ro2} \dots\dots\dots (A9)$$

$$c = c_{ro1}T_{pr} - c_{ro2} - c_{ro3}/T_{pr}^2 \dots\dots\dots (A10)$$

$$d = T_{pr} \dots\dots\dots (A11)$$

$$e = 0.6816/T_{pr}^{2} \dots\dots\dots (A12)$$

$$f = 0.6845 \dots\dots\dots (A13)$$

$$g = 0.27 p_{pr} \dots\dots\dots (A14)$$

Table 14: Values of constants that are used while using DPR method

DPR method for z factor	
$\mathbf{a_{ro}}$	0.06423
$\mathbf{b_{ro1}}$	0.5353
$\mathbf{b_{ro2}}$	0.6123
$\mathbf{c_{ro1}}$	0.3151
$\mathbf{c_{ro2}}$	1.0467
$\mathbf{c_{ro3}}$	0.5783
$\mathbf{e_{ro}}$	0.6816
$\mathbf{f_{ro}}$	0.6845

$$\rho_{pr_{new}} = \rho_{pr} \left[\frac{f(\rho_{pr})}{df(\rho_{pr})} \right] \dots\dots\dots (A15)$$

Using the new pseudodensity, another new pseudodensity is calculated Equation A7 and A8. This action is done multiple times until $f(\rho_{pr})$ becomes negligible.

$$Z = 0.27 \left[\frac{p_{pr}}{\rho_{pr} T_{pr}} \right] \dots\dots\dots (A16)$$

Gas formation volume factor canbe calculated from the following expression,

$$B_g = 0.283 \left(\frac{ZT}{p} \right) \dots\dots\dots (A17)$$

From, definition of Joule-Thomson co-efficient,

$$v = \frac{1}{\rho} \dots\dots\dots (A18)$$

$$\frac{d\rho}{dT} = df(\rho_{pr})/(\frac{1}{T_{pc}}[b_{ro1}\rho_{pr}^3 + c_{ro1}\rho_{pr}^2 + 2c_{ro3}\left(\frac{\rho_{pr}^2}{T_{pr}^3}\right) + \rho_{pr} - 2e\left(\frac{\rho_{pr}^3}{T_{pr}^3}\right)(1 + f\rho_{pr}^2)e_{pr}^{-f\rho^2} \dots\dots\dots (A19)$$

$$\left(\frac{\partial Z}{\partial T}\right)_p = -0.27\frac{p_{pr}}{T_{pr}\rho_{pr}}[\frac{1}{T} + \frac{1}{\rho_{pr}}\left(\frac{d\rho_{pr}}{dT}\right)] \dots\dots\dots (A20)$$

$$C_{JT} = \frac{1}{C_P}\left(\frac{vT}{Z}\right)\left(\frac{\partial Z}{\partial T}\right)_p \dots\dots\dots (A21)$$

Viscosity of the gas can be calculated from Lee et al (1966) method,

$$\mu_g = A(10^{-4})EXP\left(B\rho_g^c\right) \dots\dots\dots (A22)$$

$$Where, A = \frac{(9.397 + 0.01607 * MW)T^{1.5}}{209.2 + 19.26 * MW + T} \dots\dots\dots (A23)$$

$$3.448 + \frac{986.4}{T} + 0.01009 * MW \dots\dots\dots (A24)$$

$$C = 2.447 - 0.2224B \dots\dots\dots (A25)$$

APPENDIX B

Sensor Specifications For Field Case Study Data

Temperature sensor

Table 15: Temperature sensor specifications

Parameters	Specifications	Remarks
Resolution	0.0055°F	
Accuracy	±1°F	
Response	0.5 seconds	In turbulent flow

Pressure sensor

Table 16: Pressure sensor specifications

Parameters	Specifications	Remarks
Max combined error	0.02%	
Resolution	0.008 psi	
Response time	<1 sec	In turbulent flow

APPENDIX C

Spinner Flowmeter Callibration

Table 17: Spinner calibration results for Well A 39.1 MMscfD case

Zone	From (ft)	To (ft)	(+)ve slope	(+)ve Intersection
1	11676.8	11683.36	0.083	-651.159386
2	11742.4	11748.96	0.083	-618.788018
3	11794.88	11801.44	0.083	-613.392156
4	11873.6	11880.16	0.083	-613.739455
5	12004.8	12011.36	0.083	-603.471113
6	12103.2	12109.76	0.083	-577.547478
7	12162.24	12168.8	0.083	-460.797817
8	12227.84	12234.4	0.083	-409.220112
9	12300	12306.56	0.083	-349.638713

Table 18: Spinner calibration results for Well A 30.9 MMscfD case

Zone	From (ft)	To (ft)	(+)ve slope	(+)ve Intersection
1	11676.8	11683.36	0.088	-505.799684
2	11742.4	11748.96	0.088	-495.456624
3	11794.88	11801.44	0.088	-505.511776
4	11873.6	11880.16	0.088	-518.639029
5	12004.8	12011.36	0.088	-539.532246
6	12103.2	12109.76	0.088	-524.783555
7	12162.24	12168.8	0.088	-392.589609
8	12227.84	12234.4	0.088	-371.293990
9	12300	12306.56	0.088	-310.543819

Table 19: Spinner calibration results for Well A 23.5 MMscfD case

Zone	From (ft)	To (ft)	(+)ve slope	(+)ve Intersection
1	11676.8	11683.36	0.087	-422.056636
2	11742.4	11748.96	0.087	-430.531880
3	11794.88	11801.44	0.087	-440.531970
4	11873.6	11880.16	0.087	-463.933243
5	12004.8	12011.36	0.087	-512.224580
6	12103.2	12109.76	0.087	-507.334231
7	12162.24	12168.8	0.087	-379.594642
8	12227.84	12234.4	0.087	-356.833151
9	12300	12306.56	0.088	-310.543819

Table 20: Spinner calibration results for Well B 60.0 MMscfD case

Zone	From (ft)	To (ft)	(+)ve slope	(+)ve Intersection
1	11686.24	11692.8	0.253	-620.307285
2	10732.16	10738.72	0.253	-619.630025
3	10771.52	10778.08	0.253	-486.744436
4	10817.44	10824	0.253	-432.381911
5	10869.92	10876.48	0.253	-309.111669
6	10915.84	10922.4	0.253	-310.688349
7	10968.32	10974.88	0.253	-313.361266
8	11007.68	11014.24	0.253	-309.173219
9	11073.28	11079.84	0.253	-223.709387

Table 21: Spinner calibration results for Well B 40.0 MMscfD case

Zone	From (ft)	To (ft)	(+)ve slope	(+)ve Intersection
1	11686.24	11692.8	0.332	-336.856359
2	10732.16	10738.72	0.332	-337.243920
3	10771.52	10778.08	0.332	-270.241145
4	10817.44	10824	0.332	-243.056784
5	10869.92	10876.48	0.332	-156.820241
6	10915.84	10922.4	0.332	-158.649319
7	10968.32	10974.88	0.332	-160.002264
8	11007.68	11014.24	0.332	-156.962310
9	11073.28	11079.84	0.332	-101.722208

Table 22: Spinner calibration results for Well B 20.0 MMscfD case

Zone	From (ft)	To (ft)	(+)ve slope	(+)ve Intersection
1	11676.8	11683.36	0.364	-176.372941
2	11742.4	11748.96	0.364	-178.226367
3	11794.88	11801.44	0.364	-130.537631
4	11873.6	11880.16	0.364	-109.095317
5	12004.8	12011.36	0.364	-50.880165
6	12103.2	12109.76	0.364	-52.347511
7	12162.24	12168.8	0.364	-53.113684
8	12227.84	12234.4	0.364	-51.139206
9	12300	12306.56	0.364	-23.742001

Table 23: Spinner calibration results for Well C 64.0 MMscfD case

Zone	From (ft)	To (ft)	(+)ve Slope	(+)ve Int	(-)ve Slope	(-)ve Int
1	11040.48	11083.12	0.086	-506.722008	0.103	N/A
2	11119.2	11243.84	0.086	-430.201189	0.103	N/A
3	11256.96	11404.56	0.086	-125.329531	0.103	N/A
4	11420.96	11466.88	0.086	-118.115707	0.103	N/A
5	11489.84	11611.2	0.086	-11.995691	0.103	-21.016095
6	11637.44	11703.04	0.086	-9.568692	0.103	-20.451673
7	11040.48	11083.12	0.086	-3.101468	0.103	-15.844138

Table 24: Spinner calibration results for Well C 40.0 MMscfD case

Zone	From (ft)	To (ft)	(+)ve Slope	(+)ve Int	(-)ve Slope	(-)ve Int
1	11040.48	11083.12	0.078	-444.608638	0.097	-400.332004
2	11119.2	11243.84	0.078	-332.650904	0.097	-307.439683
3	11256.96	11404.56	0.078	-109.019670	0.097	-104.164445
4	11420.96	11466.88	0.078	-101.984071	0.097	-93.447590
5	11489.84	11611.2	0.078	-8.994803	0.097	-16.750559
6	11637.44	11703.04	0.078	-8.721302	0.097	-16.665949
7	11040.48	11083.12	0.078	-1.682250	0.097	-10.230092

Table 25: Spinner calibration results for Well C 28.5 MMscfD case

Zone	From (ft)	To (ft)	(+)ve Slope	(+)ve Int	(-)ve Slope	(-)ve Int
1	11040.48	11083.12	0.082	-249.071537	0.092	-249.071537
2	11119.2	11243.84	0.082	-222.134339	0.092	-188.091686
3	11256.96	11404.56	0.082	-60.957000	0.092	-59.057277
4	11420.96	11466.88	0.082	-58.846701	0.092	-58.408629
5	11489.84	11611.2	0.082	6.350875	0.092	-9.143630
6	11637.44	11703.04	0.082	8.019968	0.092	-9.311125
7	11040.48	11083.12	0.082	10.419998	0.092	1.810144